R. & M. No. 3655

MINISTRY OF AVIATION SUPPLY

AERONAUTICAL RESEARCH COUNCIL
REPORTS AND MEMORANDA

Low-Speed Wind-Tunnel Tests on a Sweptback Wing Model (Buccaneer Mark I) with Blowing at the Wing Leading Edge and Blowing over the Flaps and Drooped Ailerons

By S. F. J. BUTLER

Aerodynamics Dept., R.A.E., Farnborough

LONDON: HER MAJESTY'S STATIONERY OFFICE
1971
PRICE £1 8*s* 0*d* [£1·40] NET

Low-Speed Wind-Tunnel Tests on a Sweptback Wing Model (Buccaneer Mark I) with Blowing at the Wing Leading Edge and Blowing over the Flaps and Drooped Ailerons

By S. F. J. BUTLER

Aerodynamics Dept., R.A.E., Farnborough

Reports and Memoranda No. 3655*
September, 1967

Summary.

Low-speed longitudinal stability measurements are described on a fifth-scale half-model, including some comparisons with complete-model tests and the measured aircraft performance.

Shroud blowing over the trailing-edge flap and drooped aileron nearly doubled the C_L increment, to as much as 1·0, with adequate aileron roll control effectiveness at a mean aileron angle of up to 30°. Trimming reduced the lift increments by about 20 per cent.

Despite considerable aerodynamic objections associated with the thin wing and small nose radii, an integral (non-deflecting) leading-edge blowing arrangement was specified for aircraft structural reasons. Although an acceptable arrangement was developed, this necessitated the selection of a safe compromise position for the blowing nozzle to avoid adverse compressibility effects at aircraft take-off and landing speeds. Typically, a stalling incidence of 20° ($C_{L_{max}} = 1{\cdot}8$) was achieved for the proposed take-off configuration (30° flap; 20° mean aileron droop). With the prescribed integral leading edge, wing pitch-up at the stall was not avoided, although initial wing flow separations were confined to the inboard wing.

In general, the aircraft high-lift performance confirms the results of the tests on this half-model.

*Replaces RAE Tech. Report No. 67 223—A.R.C. 29 976.

LIST OF CONTENTS

1. *Introduction.*

The application of boundary-layer control[1] by blowing for high lift has been the subject of a series of investigations in the R.A.E. No. 2 11½ft × 8½ft wind tunnel. Model tests have been completed on slot-blowing arrangements for the De Havilland Sea Venom[2], the Saunders-Roe P.177[3], and the Supermarine Scimitar[4], as well as the experiments considered herein on an existing one-fifth scale half-model of the Buccaneer Mark I aircraft.

Exploratory investigations were first made on this model by the firm in their 7ft × 5ft tunnel at Brough, under conditions of severe tunnel constraint. The present report discusses the force and moment measurements, subsequently made in the larger R.A.E. tunnel between 1957 and 1962*, with rearward tangential blowing at the leading edge of the integral thin wing and shroud blowing over the trailing-edge flap and drooped aileron.

The effect of shroud blowing over the trailing-edge flap and drooped aileron on the basic wing characteristics and on the downwash at the tailplane is considered first, in the absence of leading-edge devices. The effect of local nozzle blockage representing typical flap and aileron support gear, and the effects of the presence of the main undercarriage and the airbrake are also presented.

The main discussion concerns the development and optimisation of a suitable leading-edge slot-blowing arrangement. For structural reasons, a leading-edge flap with blowing at the knuckle could not be incorporated on the aircraft, although clearly preferable from aerodynamic considerations. With the thin wing section (typically 8 per cent RAE 101, with some added nose camber), the prescribed integral leading-edge arrangement (i.e. no movable surfaces) was inevitably associated with high negative pressure peaks and severe adverse pressure gradients under high lift conditions. Even at the comparatively low main-stream Mach number ($M \approx 0{\cdot}2$) representative of aircraft take-off and landing conditions, the local peak velocity approached sonic conditions.

Under these circumstances, the effectiveness of the leading-edge blowing arrangement was found to depend not only on chordwise location but also on the main-stream Mach number and nozzle pressure ratio, thus necessitating the choice of a safe compromise arrangement for the aircraft.

Some comparisons are presented between the test results obtained on this half-model, and on the 1/12th-scale complete model used by the firm for general stability and performance measurements. A flight-tunnel comparison is also included.

2. *Model Details.*

The one-fifth scale port-wing half-model was originally constructed by H.S.A. (Brough) for tests in their 7ft × 5ft low-speed tunnel. For the present tests, it was mounted on the virtual-centre lower balance of the R.A.E. No. 2 11½ft × 8½ft wind tunnel (*see* Figs. 1 and 2). The model was made mainly from wood, except for the mounting brackets, blowing ducts and nozzles, which were constructed from steel, duralumin, and brass.

Prior to the R.A.E. tests, the model was modified (*see* Figs. 1 and 2) to be more representative of the Buccaneer Mark I aircraft. In particular, the fuselage was lengthened, with provision for representation of the petal-type airbrake at the rear of the fuselage and the main undercarriage. A flat-plate fin was provided, to support the half-tailplane when fitted; the all-moving tailplane incorporated a trimming flap, but the aircraft tailplane leading-edge blowing arrangement was not represented. As previously, free flow was allowed through the simulated main engine nacelle duct.

The wing, of full aspect ratio 3·55 and taper ratio 0·59 had a constant trailing-edge sweepback of 20 ; the quarter-chord sweepback was 30·2° over most of the exposed span, increasing progressively to 38·6° inboard of the wing planform blend region (*see* Fig. 1). The wing, which had zero twist, was mounted at a mid-fuselage position, with zero dihedral and +2·5° wing-fuselage angle. The wing section varied across the span, with a 9·25 per cent thick RAE 100 symmetrical section at the fuselage centreline, an 8 per cent thick RAE 101 section with nose camber at 55 per cent semi-span, and a 6 per cent thick RAE 102 section with nose camber at the tip: typical nose profiles are shown in Fig. 4.

*The test results were analysed at the time and received a limited circulation in the form of H.S.A. (Brough) internal reports.

The wing trailing-edge flap and large-span aileron (*see* Fig. 1 and Table 1), which were supported by lower surface brackets providing arbitrarily prescribed angular settings of up to 75° and 45° respectively (normal to hinge-line), were generally representative of the aircraft arrangement, with round-nosed controls centrally-hinged at about 76 per cent wing chord (*see* Fig. 3a). In addition to the leading-edge blowing arrangements for the integral wing nose, provision was made (*see* Table 1) for a leading-edge slat (*see* Fig. 12), with 15 per cent chordwise area extension and 15° angular setting, and a leading-edge flap hinged at 15 per cent chord on the wing lower surface with 30° deflection (normal to hinge-line).

The wing was fitted with two full-span main air ducts (*see* Fig. 1) conveying the high-pressure air to nozzles at the wing nose and in the wing shroud ahead of the trailing-edge flap and aileron. The shroud-blowing installation was conventional (*see* Fig. 3a), with the nozzle parallel to the wing chord plane and the lower face of the nozzle aligned tangentially with the nose of the flap and the aileron. Usually, the nozzle depth was regulated by small spacers at 2-inch intervals across the span. To simulate the effect of proposed flap and aileron support-gear arrangements, alternative larger-span spacers were provided to seal the appropriate sections of the nozzle span.

For aircraft design reasons, the inboard limit of the leading-edge blowing nozzle was determined by the wing fold at 44 per cent semi-span. The leading-edge blowing arrangement originally tested by H.S.A. (Brough), provided a nozzle at 5 per cent chord, inclined at about 30° to the local wing surface (*see* Fig. 3b). For the initial R.A.E. tests, additional nozzles at $1\frac{1}{2}$ per cent–2 per cent chord (with tangential ejection) were arranged by the addition of auxiliary brass nose-plates, with small spacers to regulate the nozzle depth (*see* Fig. 3c). In addition, a nozzle at $\frac{1}{4}$ per cent chord was contrived by the use of a further brass nose plate incorporating a series of nozzles formed by saw-cuts inclined at about 30° to the local surface (Fig. 3d). For the final R.A.E. tests, a single nose unit was manufactured incorporating two alternative nozzles (at $\frac{1}{4}$ per cent and $1\frac{1}{2}$ per cent chord), each nozzle inclined at 30° to the local surface (Figs. 3e and 3f). The nozzle depth was regulated by internal spacers upstream of the final contraction, so that the actual nozzles were unobstructed. By the careful use of a stiff Araldite mixture of minimum adhesive strength, it was possible to seal and open each nozzle in turn, as desired.

Most of the tests were made at 200 ft/sec, corresponding to a Reynolds number of $3{\cdot}0 \times 10^6$ based on standard mean chord, but the speed was reduced to 140 ft/sec for certain tests at reduced Mach number. Throughout, transition was left free on the wing and the tailplane, but fixed on the fuselage nose.

3. *Test Procedure.*

3.1. *The Effect of Blowing Air Supply on Balance Zeros.*

For the first series of tests at R.A.E., a similar air supply arrangement[5] was adopted as for the earlier blowing tests[2,3,4], using a canvas-sleeve necked connector. For the later tests, the air connection was effected by an air-bearing connector[6]. The zeros for blow-on runs were taken with the appropriate static-pressure conditions in the connectors. The zero scatter was not appreciably greater than that which would have occurred with a conventional (unblown) model on this balance.

3.2. *Specification of Blowing Momentum Coefficient.*

The gross blowing momentum coefficient, C_μ, was defined[5] in terms of the measured mass-flow rate, and the theoretical velocity after isentropic expansion to free-stream static pressure (*see* List of Symbols). Spanwise traverses of nozzle total head were made (*see* Fig. 5) to determine mean values from which the let velocity could be calculated. The momentum-coefficient values obtained from the measured mass-flow rate and jet velocity were consistent with the slightly larger values derived from the nominal nozzle area and the jet velocity.

Suffices have been used to distinguish between nose blowing (C_{μ_N}) and rear shroud blowing (C_{μ_R}). Mean sectional coefficients, C'_{μ_N} and C'_{μ_R} were defined likewise, with the gross wing area replaced by the area, S', of the wing corresponding to the span of the blowing nozzle. Thus:

$$C'_{\mu_N} = C_{\mu_N} \frac{S}{S'_N} = 2{\cdot}6\, C_{\mu_N} \text{ for the final leading-edge arrangement}$$

$$C'_{\mu_R} = C_{\mu_R} \frac{S}{S'_R} = 1{\cdot}55\, C_{\mu_R}.$$

For the available pressure ratio of about 3:1, the maximum values of C_{μ_N} and C_{μ_R} were approximately 0·045, 0·07 respectively (each corresponding to sectional values of about 0·11), at the usual test speed of 200 ft/sec. For the aircraft, engine thrust considerations restricted the value of $(C_{\mu N} + C_{\mu R})$ to 0·065 for the take-off configuration.

The nozzle width was varied spanwise, broadly in proportion to the local wing chord, and the nozzle total head did not vary much across the span of each nozzle (*see* Fig. 5). Thus, the local sectional momentum coefficient sensibly remained equal to the mean sectional momentum coefficient across the span of each nozzle.

3.3. *Corrections.*

In addition to the usual allowances for solid blockage, suitable corrections have been applied to allow for increased wake blockage when flow separations are present[7]. The resulting changes in the nominal test values of mainstream dynamic head, $\frac{1}{2}\rho_0 V_0^2$, amounted to 2 per cent–3·5 per cent (at or below the stall) and up to 12 per cent (above the stall).

The following tunnel constraint* corrections were added subsequently:

$$\Delta\alpha_{\text{degrees}} = 0{\cdot}837\, C_{L_{\text{no tailplane}}}$$

$$\Delta C_{D_c} = 0{\cdot}0145\, C^2_{L_{\text{no tailplane}}}$$

$$\text{(Tailplane-on runs) } \Delta C_{m_c} = -0{\cdot}435 \left(\frac{dC_m}{d\eta_T}\right) C_{L_{\text{no tailplane}}} (\eta_T \text{ in degrees}).$$

To assist direct comparison with the firm's model tests for this aircraft, the pitching-moment coefficients have been based on the standard mean chord $\bar{c}$, rather than the aerodynamic mean chord $\bar{\bar{c}}$, and have been referred to $0{\cdot}25\,\bar{\bar{c}}$ $\left(\text{N.B.}\ \frac{\bar{c}}{\bar{\bar{c}}} = 0{\cdot}946\right)$.

4. *Tests with Shroud Blowing over the Trailing-Edge Flap and Drooped Aileron, without Leading-Edge Devices.*

4.1. *Scope.*

In the preliminary tests by the firm in their 7ft × 5ft tunnel, the effect of trailing-edge shroud blowing over the flap and aileron was studied in some detail. Although these tests were subject to quite large tunnel constraint effects, by normal research standards, useful results were nevertheless obtained at low incidences. Consequently, the R.A.E. tests were mainly confined to a confirmation of the general effects of shroud blowing under conditions of reduced tunnel constraint (Sections 4.2, 4.3, and 4.4). In addition, it was now feasible to make measurements of mean downwash at the tailplane (Section 4.4). For these tests, a standard model configuration was adopted, with the fin plate present, the tailplane off (unless otherwise specified), the airbrake retracted, and the undercarriage assembly removed. The basic undeflected wing leading edge was used, without leading-edge blowing. The shroud nozzle was unobstructed, except for small, regulating spacers.

The effect of partial nozzle blockage, representing possible obstruction by aircraft flap and aileron support gear, was simulated for certain representative cases (Section 4.5). Finally, a few tests were made with the petal-type air-brake at the rear of the fuselage fully extended, and with the main undercarriage assembly added (Section 4.6).

*The corresponding corrections for the exploratory tests by the firm were some three times this size (S/C = 0·34, compared with 0·11 for the R.A.E. tests).

4.2. *Lift.*

The position of the wing fold relative to the exposed wing severely limited the spanwise extent of the aircraft flap inboard of the fold, while practical design considerations favoured the use of a large-span constant deflection aileron outboard of the fold. In order to meet the take-off and landing lift requirements, therefore, mean droop was applied to the aileron, together with the usual provision for differential movement of the ailerons for roll control, within the overall design deflection limit of about 45°. Consideration of rolling control requirements suggested a provisional limit of 30° on mean aileron droop, on the assumption that blowing B.L.C. would ensure a reasonable contribution to rolling moment from the down-going aileron with this value of mean droop (*see* Section 4.5 and Appendix B).

The general effect of shroud blowing over the flap and the drooped aileron is shown in Fig. 6 for representative flap and aileron settings. At the lowest C_{μ_R}-values examined ($C_{\mu_R} = 0{\cdot}020$, equivalent to $C'_{\mu_R} = 0{\cdot}032$), tufts indicated that attached flow was achieved over most of the span of the controls, as would be expected in view of the increase of 60 per cent to 80 per cent in the effectiveness of the combined flap and aileron, relative to the unblown condition. Thus, the value of $C_{\mu_R} = 0{\cdot}04$ proposed for the aircraft was sufficient to ensure well-attached flow, with adequate safety margins. Further increases in lift at constant incidence would naturally result from larger values of C_{μ_R}, but at a reduced rate (*see* Fig. 6). Moreover, comparable lift increment increases could be achieved anyway with leading-edge blowing* (*see* Section 5.4), with additional beneficial effects on stalling incidence and $C_{L_{max}}$.

Because of the span of the flap, the variation of lift with flap angle at a prescribed value of C_{μ_R} (Fig. 8a) was inevitably small, compared with the corresponding variation with aileron angle (Fig. 9a). In addition, tufts showed that completely attached flow could not be achieved on the small-span flap, particularly at large flap angles. Thus, from the point of view of lift, the optimum flap angle was rather low, about 45° (*see* Fig. 8a), compared with previous experience on larger-span inboard flaps[2,3,4].

In the choice of the aircraft take-off configuration, engine thrust considerations necessitated a compromise between the conflicting requirements for high lift and low drag (*see* Section 4.3). Thus, the flap and mean aileron droop settings were initially limited to 30° and 20° respectively. For landing the corresponding settings of 45° and 30° ensured higher lift, with the retention of adequate aileron effectiveness for roll control with the basic uninterrupted blowing nozzle (*see* Fig. 9a and Section 4.5).

With the application of the appropriate aspect ratio and part-span lift conversion factors, the experimental lift increments compare reasonably well with the corresponding results for a similar configuration (S.R. 177) with shroud blowing over the flap and the aileron (*see* Fig. 33b of Ref. 3).

Because of the magnitude of the nose-down pitching-moment changes due to the blown flap and aileron, and the short tail-arm, the associated trimming losses were appreciable. Typically, for $\beta = 30°$, $\xi = 20°$ and $C_{\mu_R} = 0{\cdot}04$, the lift penalty amounted to $\Delta C_{L_t} = -0{\cdot}14$, about 20 per cent of the lift increment due to the flap and drooped aileron (*see* Section 4.4 and Fig. 11).

4.3. *Drag.*

The general effect of shroud blowing on the C_D v. C_L (no tail) curves is shown in Fig. 7, for representative settings of the flap and drooped aileron. The variation of drag with flap angle and with aileron angle is shown in Figs. 8b and 9b respectively, for prescribed values of C_{μ_R}. The measured drag coefficients include any jet thrust which may be recovered.

For the unblown flap and aileron, the drag penalty at a constant low C_L-value increased with flap and aileron angle, amounting to about $\Delta C_D = +0{\cdot}02$ at $\beta = 30°$, $\xi = 20°$. At such moderate control angles, the reduction in C_D at constant C_L due to blowing was nearly equal to the applied value of C_{μ_R}. However, at higher deflections, there was a net penalty associated with the application of blowing as well as a higher ΔC_D for the unblown case. Thus, significant variations in drag occurred as the angle of the small-span blown flap was varied, although the corresponding lift changes were small (*see* Figs. 8a and 8b). The corresponding variation of drag with aileron setting (*see* Fig. 9b) would be expected to result in significant yawing moments, on the application of aileron differential in the presence of shroud blowing.

*Assuming a limitation on the total values of $C_{\mu_N} + C_{\mu_R}$ of 0·065.

The variation of C_D with C_L^2 remained essentially linear over a wide incidence range (*see* Fig. 7d), with the value of $\pi A \frac{dC_D}{dC_L^2}$ decreasing significantly with deflection of trailing-edge controls and application of blowing from 1·26 (flaps up) to 1·15 ($\beta = 45°$, $\xi = 30°$, $C_{\mu_R} = 0{\cdot}04$).

As usual, there was a need to optimise the flap/aileron blowing configuration at take-off, to minimise drag. For the landing configuration, additional drag could be provided, with beneficial reductions in minimum drag speed, by suitable increases in the difference between the flap angle and the mean aileron droop angle[1,3,4].

4.4. *Pitching Moments and Downwash at the Tailplane.*

Pitching moments are referred to the test *cg* at 0·25 $\bar{c}$ on the wing chord plane and the fuselage datum. To facilitate direct comparison with tests by the firm, the pitching-moment coefficients have been referred to standard mean chord $\bar{c}\left(\frac{\bar{c}}{\bar{\bar{c}}} = 0{\cdot}946\right)$. The general effect of shroud blowing on the C_m v. C_L curves is shown in Fig. 7 for various flap and aileron settings. A few representative curves are given with the tailplane present, including tests with the tailplane trimming flap deflected.

Deflection of the flap and drooped aileron, together with the application of shroud blowing, resulted in the expected nose-down pitching-moment changes for the wing without the tailplane. Because of the difference in span and the sweepback of the control hinge-line, the variation of pitching moment with flap angle (Fig. 8c) was naturally much smaller than the corresponding variation with mean aileron droop (Fig. 9c). The pitching-moment and lift increments due to mean aileron droop were proportional, so that the application of aileron differential for roll control would not be expected to result in large pitching-moment variations at a given mean aileron deflection.

An increase in static stability generally resulted from the application of blowing in the absence of the tailplane, together with an increase in the severity of the wing pitch-up at the stall. The variation of mean downwash at the tailplane (Fig. 10) was deduced from comparison of results with and without the tailplane. The application of blowing increased the downwash at the tailplane by about 2°, slightly increased the tailplane contribution to static stability, but did not seem to affect the tailplane power $\left(\frac{dC_m}{d\eta_t} \sim -0{\cdot}012 \text{ per degree}\right)$ to a significant extent; in most cases, there was a gradual reduction of the tailplane power with increasing incidence.

The magnitude of the nose-down pitching-moment increments due to the blown flap and drooped aileron, together with the small tail arm (1·96 $\bar{c}$), necessitated combined use of an all-moving tailplane and a tailplane flap for trimming. The associated lift losses due to trimming were appreciable. Thus, with $\beta = 30°$, $\xi = 20°$ and $C_{\mu_R} = 0{\cdot}04$ (the original aircraft take-off configuration), the loss amounted to $\Delta C_{L_t} = -0{\cdot}14$ with the *cg* at 0·32 $\bar{c}$ (*see* Fig. 11), some 20 per cent of the total lift increment due to flap and drooped aileron.

The present tests showed a maximum tailplane increment (with tailplane flap deflected) of about $\Delta C_{m_t} = 0{\cdot}4$, followed by a gentle tailplane stall (*see* Fig. 7). At a higher Reynolds number, with leading-edge blowing on the tailplane as well as a trimming flap, other tests suggested that the aircraft tailplane should achieve at least a $C_{L_{max}}$ of $-1{\cdot}5$ (based on tailplane area), corresponding to $\Delta C_{m_t} = 0{\cdot}44$ and $\Delta C_{L_t} = -0{\cdot}22$. The aircraft *cg* limits were chosen accordingly, to ensure an adequate margin against the possibility of an inadvertent tailplane negative stall at high lift. Also, the negative tailplane movement available (some $-20°$ selative to datum) was adequate to allow trimming throughout the usable incidence range. At the rearmost *cg* contemplated (0·32 $\bar{c}$), the static stability margin was about 0·08 $\bar{c}$ in a typical case.

4.5. *The Effect of Local Nozzle Blockage, Representing Flap and Support Gear.*

The effect of partial nozzle blockage, representing the possible obstructions caused by proposed aircraft arrangements for the flap and aileron support gear, was determined by introducing wide spacers into the shroud blowing nozzle at the appropriate spanwise positions. At model scale, three 0·48-inch

wide spacers were inserted across the span of the aileron and one 0·32-inch wide spacer opposite the flap. Altogether, this blockage amounted to only a 4 per cent reduction in total nozzle area. The shroud blowing pressure was increased by a suitable amount to restore the original value of C_{μ_R}.

The detrimental effect of such blockage increased at large deflection angles (Fig. 9), as found previously[3]. Particularly serious was the implication of an almost complete loss of effectiveness for roll control* of the downward-moving aileron, for the proposed aircraft landing configuration with a mean aileron droop of 30°. Consequently, a partially successful attempt was made to modify the design of the flap and aileron gear to minimise such interruptions of the shroud nozzle on the aircraft.

To achieve maximum benefit from a B.L.C. blowing installation, it is essential to minimise discontinuities in the blowing nozzle efflux, or in the upper surface contour of the deflected controls[2].

4.6. *The Effect of the Airbrake and the Main Undercarriage Assembly.*

The addition of the main undercarriage assembly (with or without the door) caused a reduction in lift at constant incidence. The lift loss increased with C_{μ_R}, amounting to $\Delta C_L = -0{\cdot}07$ for the take-off configuration $\beta = 30°, \xi = 20°, C_{\mu_R} = 0{\cdot}04$; the loss with $\beta = 60°, \xi = 30°, C_{\mu_R} = 0{\cdot}04$ was similar in magnitude. In either case, the associated drag increment at constant C_L amounted to $\Delta C_D \simeq 0{\cdot}02$. The overall trim changes were small, as the positive no-tailplane pitching-moment increment ($\Delta C_m \simeq +0{\cdot}03$) was accompanied by a reduction in downwash at the tailplane.

Extension of the petal-type airbrakes (with strakes) did not cause any appreciable changes in lift. The drag increment at constant C_L amounted to $\Delta C_D \simeq 0{\cdot}09$. There was also a small nose-down pitching-moment increment, $\Delta C_m \simeq -0{\cdot}02$, with and without the tailplane present, for the cases examined.

a. Tests with Leading-Edge Devices.

5.1. *Scope.*

Although the preliminary tests in the 7ft × 5ft tunnel included extensive stalling investigations, these were necessarily exploratory in nature in view of the magnitude of the tunnel constraint corrections and the possibility of unrepresentative effects on the stalling behaviour (*see* Appendix A).

For comparative purposes, a few preliminary tests (Section 5.2) were made at R.A.E. with some existing conventional mechanical high-lift leading-edge devices, including a part-span leading-edge slat with chord extension, and a part-span leading-edge flap. However, the main tests (Sections 5.3 and 5.4) concerned the development and optimisation of a suitable B.L.C. blowing arrangement for the prescribed aircraft *integral*† leading-edge configuration. For the present compasatively thin wing (typically 8 per cent R.A.E. 101 streamwise, with some local added nose camber), this involved not only the determination of the best blowing nozzle position, and detailed modifications to the wing nose shape, but also the investigation of mainstream Mach number effects.

5.2. *Preliminary Tests with Mechanical Leading-Edge Devices.*

The results of brief tests on an existing leading-edge slat arrangement are summarised in Fig. 12. This slat, which only extended from 55 per cent semi-span to the wing tip, provided an average chordwise extension of some 15 per cent and was set at 15° deflection.

For the various flap and aileron configurations without trailing-edge shroud blowing ($C_{\mu_R} = 0$), the addition of the slat improved $C_{L_{max}}$ and substantially delayed the onset of stall, relative to the basic undeflected and unblown wing nose. At the higher rear loadings which occurred with shroud blowing over the trailing-edge flap and drooped aileron, however, this part-span slat did not improve $C_{L_{max}}$ because of inboard wing flow separations. However, the severity of the post-stall lift losses were reduced because of

*It is necessary to assume, with a half model, that the effectiveness of aileron differential for roll control can be inferred from tests with a range of symmetrical droop settings.

†Although superior and mose straightforward aerodynamically (*see* Section 5.2) the alternative of a leading-edge flap with B.L.C. at the knuckle was not investigated, being rejected as unacceptable for structural reasons in the present case.

the improved outer-wing flow, and there was some alleviation of the severity of the pitch-up. No attempt was made to improve the slat arrangement, or to vary its spanwise extent.

Further experiments, with a simple unblown deflected leading-edge flap (no area extension) on the outer part of the wing span produced results generally resembling those obtained for the part-span slat, the stall starting either on the inboard wing or at the junction with the leading-edge flap. Better results were obtained with the leading-edge flap extended inboard, the results from the most promising configuration being summarised in Fig. 13. Here, the unblown leading-edge flap extended from 32 per cent semi-span to the tip, with 30° deflection normal to the κinge-line (on the wing lower surface). Over the outer part of the wing, the hinge-line was at 15 per cent chord, but due to the increased leading-edge sweepback the flap chord was appreciably greater at the inboard end of the flap. To achieve the results shown in Fig. 13, a nose fence was necessary at the inboard end of this flap.

In the presence of shroud blowing over the trailing-edge flap and drooped aileron, this leading-edge flap was (not surprisingly) more effective than the part-span slat specifically considered. Thus, for the proposed aircraft take-off configuration ($\beta = 30°, \xi = 20°, C_{\mu_N} + C_{\mu_R} = 0{\cdot}065$), deflection of the leading-edge flap resulted in significant improvements in $C_{L_{max}}$ and stalling incidence, admittedly with some reduction in lift at constant incidence. The wing now stalled as the result of flow separations from the knuckle of the leading-edge flap, rather than the wing nose.

As tested, however, even the large-span unblown leading-edge flap only just achieved the minimum objective ($C_{L_{max}} \geqslant 1{\cdot}8, \alpha_{stall} \geqslant 20°$) for the psoposed take-off arrangement. Moreover, *any* kind of non-integral wing leading-edge arrangement was considered unacceptable for structural reasons in the present case. Almost certainly, had this not been so, the leading-edge flap arrangement tested could have been developed by the incorporation of a suitable B.L.C.[1,9,10] arrangement at the leading-edge knuckle, to exceed the above objective by an appreciable margin, thus allowing more consideration of stall and post-stall characteristics.

5.3. *Tests with First Integral Leading-Edge Blowing Assembly.*

Engine thrust considerations at take-off led to the initial restriction of flap and mean aileron droop to $\beta = 30°, \xi = 20°$, and also to an overall limit on blowing rate of $C_{\mu_N} + C_{\mu_R} \leqslant 0{\cdot}065$. Considerations of the relative contributions of trailing-edge blow and leading-edge blow in relation to the specified minimum aerodynamic objective ($C_{L_{max}} \geqslant 1{\cdot}8, \alpha_{stall} \geqslant 20°$), together with the results of preliminary tests by the firm and the R.A.E. tests without leading-edge devices, suggested that about 60 per cent of the available blowing air (*see* Section 4.2) should be applied at the trailing-edge ($C_{\mu_R} = 0{\cdot}04$) and the remainder at the leading edge ($C_{\mu_N} = 0{\cdot}025$). This ratio between nose and rear blowing rates was used provisionally for the tests described in this section. However, the nose and rear rates were subsequently varied individually during the final check tests described in Section 5.4.

The original leading-edge blowing assembly, as designed and tested by the firm for the integral-nose aircraft installation, entailed a nozzle at 5 per cent chord, extending from 47 per cent semi-span (determined by wing-fold position at 44 pes cent semi-span) to the wing tip. Considerations of the peak suction position at high incidences led to the provision of alternative nozzle positions at 2 per cent, $1\frac{1}{2}$ per cent and $\frac{1}{4}$ per cent chord for the R.A.E. tests on this assembly. As explained earlier (*see* Section 2), this involved the judicious use of carefully-formed metal nose fairings incorporating the required nozzles (*see* Fig. 3). Although tangential jet efflux was arranged for the $1\frac{1}{2}$ per cent and 2 per cent chord nozzles, the $\frac{1}{4}$ per cent nozzle and the original 5 per cent chord nozzle were inclined at about 30° to the local wing surface.

Because of the sensitivity to local nose shape, it proved rather difficult to achieve identical stalling behaviour for the different leading-edge nozzle arrangements at $C_{\mu_N} = 0$. Although partly due to the small nose radii involved (6 per cent R.A.E. 102 at wing tip), such difficulties were aggravated by the complexity of the wing planform and section variations in the vicinity of the nose. The basic, solid leading-edge arrangement regarded as a datum generally proved superior to the modified leading-edge blowing assembly in the absence of leading-edge blowing* (*see* Fig. 14). Particularly in the case of the $1\frac{1}{2}$ per cent

*Check tests with the leading-edge nozzles sealed and faired confirmed that these datum variations were associated with wing contour variations rather than local nozzle flows.

chord nozzle, it was found necessary to improve the nose shape, in order to restore the original contour (*see* Fig. 4) and to achieve a datum behaviour at $C_{\mu_N} = 0$ comparable with the basic leading edge. The resulting arrangement, C_3, was preferred to C_1 and C_2.

The three configurations A_1, B_1 and C_3, with nozzles at 5 per cent, 2 per cent and $1\frac{1}{2}$ per cent chord respectively, exhibited similar characteristics at $C_{\mu_N} = 0$ (*see* Fig. 14), the wing stalling as the result of the spread of leading-edge separations chordwise and spanwise from the outer wing nose. There was a progressive improvement in the effectiveness of leading-edge blowing as the nozzle position was moved forwards. In fact, for configuration C_3 with leading-edge blowing ($C_{\mu_N} = 0{\cdot}024$), the onset of wing stall was now determined by separations originating inboard of the leading-edge blowing nozzle, so that any further improvements necessitated inboard wing modifications.

The possible scope for such modifications was severely restricted by considerations of cruising drag and by structural limitations, as well as by the desirability of preserving a root stall, and ensuring some delay in the spread of the stall to the outer wing. The modification adopted, configuration C_4 (*see* Fig. 4), resulted in a small further improvement in $C_{L_{\max}}$ and stalling incidence (*see* Fig. 14c) in the presence of leading-edge blowing. This modification was retained for the tests with the $\frac{1}{4}$ per cent chord nozzle. However, some detailed improvements in contour were again found desirable, resulting in configuration D_2.

The preferred configurations A_1, B_1, C_4 and D_2 have been used to illustrate the combined effect of nozzle position and C_{μ_N} on the C_L v. α_w curves (Fig. 15). Here, the basic solid leading edge has been taken as the standard datum at $C_{\mu_N} = 0$. In general, there was a progressive improvement in stalling incidence and $C_{L_{\max}}$ as the leading-edge nozzle position was moved forwards towards the nose. Part of the increase in $C_{L_{\max}}$ was the result of increased lift at constant incidence, due to improvements in the wing boundary-layer condition in the vicinity of the trailing-edge flap and drooped aileron which resulted from the application of leading-edge blowing.

With the exception of the $\frac{1}{4}$ per cent chord nozzle, the results correlated in the normal way, with progressive increases in stalling incidence as the value of C_{μ_N} was increased. However, the results with the $\frac{1}{4}$ per cent chord nozzle at the normal test speed of 200 ft/sec showed a different trend (Fig. 15d), with progressive reduction of stalling incidence and $C_{L_{\max}}$ as C_{μ_N} was increased from 0·012 to 0·024 and 0·040. When the test speed was reduced to 140 ft/sec, the usual variation with C_{μ_N} was achieved. Similar results were found with the other $\frac{1}{4}$ per cent chord nozzle configuration, D_1. At the higher test speed, wing tufts showed that a premature flow separation from the outboard wing leading edge occurred at the higher values of C_{μ_N}. The variations of C_{μ_N} were necessarily achieved as usual by variation of nozzle pressure ratio at a prescribed gap size, so that the flow breakdown appeared to increase in severity as the pressure ratio was increased. For the aircraft application, even higher pressure ratios were contemplated, and thus more adverse compressibility effects seemed possible.

Provisionally, it was decided to locate the aircraft nozzle at $1\frac{1}{2}$ per cent chord, to avoid such effects. On comparison of Fig. 15c and Fig. 13a, it is apparent that this blowing arrangement for an integral wing was generally comparable in performance with the conventional unblown deflected leading-edge flap, at the prescribed take-off value of $C_{\mu_N} + C_{\mu_R} = 0{\cdot}065$. Typical drag and pitching-moment data for the chosen leading-edge blowing arrangement are given in Fig. 16, which confirms the general effectiveness of leading-edge blowing in delaying the onset of the stall. However, it should be noted that the application of leading-edge blowing, although ensuring a stall emanating from the inner wing, did not preclude a wing pitch-up. This resulted from the large loss of lift over the rear of the wing whenever significant flow separations were present at the wing leading edge.

As discussed earlier (Section 4.4), the aircraft *cg* range had to be chosen to avoid a negative tailplane stall at a high lift. Some margin was therefore allowed from the available trimming moment increment of 0·44 with tailplane flap deflected.

Further general indications of the rather critical nature of the wing leading-edge shape, together with a possible explanation of the apparent adverse compressibility effects with the $\frac{1}{4}$ per cent chord nozzle, are given by some leading-edge pressure distributions at 75 per cent semi-span (*see* Figs. 17 and 18). With the basic unblown leading edge, a pressure coefficient of about -10 was achieved, compared with a value of only -7 (for a reduced stalling incidence) for one of the $\frac{1}{4}$ per cent chord nozzle arrangements at $C_{\mu_N} = 0$

(Fig. 17). On the application of leading edge blowing ($C_{\mu_N} = 0{\cdot}024$) at the lower test speed of 140 ft/sec, the value of the pressure coefficient which could be achieved was now about -22 (Fig. 18), compared with the critical value ($C_p^* = -42$) for local sonic flow at this mainstream speed. However, at the higher test speed of 200 ft/sec ($M = 0{\cdot}18$) the onset of premature leading-edge flow separations limited the pressure coefficient to only -15, compared with $C_p^* = -20$. Comparable compressibility effects have been encountered in two-dimensional tests of a blown cylinder at low mainstream Mach numbers[8].

Thus, the location of the blowing nozzle at, or very close to, the minimum pressure position appeared to result in flow separations if the jet efflux induced local supersonic regions in the airflow around the nose. It is not known whether such flow separations emanated from the main wing nose ahead of the nozzle, or whether they resulted from the breakdown of the 'Coanda' effect, which was relied upon to turn the inclined jet efflux through a moderate angle (about 30°) to flow tangentially rearwards over the main wing surface. From this point of view, it should be noted that the rear face of the $\frac{1}{4}$ per cent chord nozzle was finished with a large radius to blend with the local external surface and assist the turning process.

5.4. *Tests with Second Integral Leading-Edge Blowing Assembly.*

Although a provisional decision was taken to fit a $1\frac{1}{2}$ per cent chord nozzle to the aircraft, confirmatory tests were obviously advisable, with a leading-edge unit which accurately represented the final aircraft $1\frac{1}{2}$ per cent chord nozzle design arrangement. At the same time, it was desired to effect a more satisfactory comparison between the chosen $1\frac{1}{2}$ per cent chord nozzle and the more critical $\frac{1}{4}$ per cent chord nozzle. Accordingly, a second leading-edge assembly was constructed by the firm incorporating two alternative nozzles, each nozzle inclined at 30° to the local surface (*see* Fig. 3). Arrangements were made for the sealing by choice of either, or both, of these nozzles, each of which was unobstructed by spacers along its length (*see* Section 2). Although the nozzle depth was somewhat reduced for this leading-edge, the aircraft nozzle depth/chord ratio was still not fully represented.

The wing leading-edge contour was carefully constructed to Mark I aircraft production design. It was not found feasible to incorporate on the aircraft the full inboard wing modification, as used for configurations C_4 and D_2 in the earlier tests, except in the vicinity of the wing break (*see* Fig. 4). Nevertheless, there was a close comparison between the performance of configuration C_4 and the $1\frac{1}{2}$ per cent chord nozzle of the second leading edge (*see* Fig. 19). It can be seen that the latter arrangement was slightly inferior, in terms of $C_{L_{max}}$, in the presence of leading-edge blowing, probably as a result of the differences between the inboard leading-edge geometry noted above. On the other hand, the variations of C_L above the stall were less pronounced on the second leading-edge assembly, probably as a result of the improved outboard wing contour accuracy and a more refined nozzle design. Certainly, the spanwise rate of spread of the inboard wing stall in the presence of leading-edge blowing was much reduced, as can be judged from Fig. 20. It is also interesting that the hysteresis, as determined by static tests with increasing and decreasing wing incidence, was not pronounced. In fact, usually the value of $C_{L_{max}}$ was not affected, although there were small changes in the lift coefficient at a given post-stall incidence. Figs. 20 and 21 show that further gains in $C_{L_{max}}$ would be expected to result from increase in the mean aileron droop angle at take-off, without unacceptable adverse effects on aircraft drag characteristics. The direct variation with C_{μ_N} is shown in Figs. 22 and 23, at a constant value of C_{μ_R}. The favourable effect of leading-edge blowing on the boundary-layer condition at the trailing-edge controls is shown clearly. On comparison with Fig. 6, leading-edge blowing is seen to be nearly as efficient as trailing-edge shroud blowing in producing supercirculation lift increments.

The general effect of aileron differential on wing stalling incidence and the variation of aileron roll control power with incidence and $(C_{\mu_N} + C_{\mu_R})$ can be inferred from Fig. 24. The favourable influence of blowing on aileron power was maintained up to the stall. However, the wing stalling incidence fell as the aileron was deflected and the post-stall lift losses increased. Tufts showed that the wing still stalled from the root.

A detailed comparison between the chosen aircraft nozzle position at $1\frac{1}{2}$ per cent chord and the alternative $\frac{1}{4}$ per cent chord nozzle position is given in Figs. 25 and 26. Even with the $1\frac{1}{2}$ per cent chord nozzle, minor adverse compressibility effects were found (Fig. 25d). However, these effects were much more pronounced for the $\frac{1}{4}$ per cent chord nozzle (Figs. 25 a–c), particularly with a discontinuity between the

rear face of the nozzle and the external surface of the aerofoil. The adverse compressibility effects, as shown by the difference in the behaviour at the two test speeds, were once again found to increase with C_{μ_N}. Considerable alleviation was obtained by blending the rear face of the nozzle with the aerofoil surface (*see* Fig. 3f) to assist the turning process. Nevertheless, the performance of the blended $\frac{1}{4}$ per cent chord nozzle still remained markedly inferior to that of the $1\frac{1}{2}$ per cent chord nozzle at the higher test speed. The precise mechanism of this phenomenon is still not understood.

The results at the lower speed showed that the $\frac{1}{4}$ per cent chord nozzle would be superior in the absence of such compressibility effects. Thus, the post-stall lift loss was postponed to much higher incidences and the margin between the stall of the unblown inner wing and the stall of the blown outer wing was increased correspondingly. This was confirmed by some wing tuft studies of the incidence at which leading-edge separations occurred on the outer wing (Fig. 26). In the absence of compressibility limitations, at the lower speed, the $\frac{1}{4}$ per cent chord nozzle resulted in smaller minimum values for C'_{μ_N} and much higher sectional stalling incidences. The chosen $1\frac{1}{2}$ per cent chord nozzle was much inferior at this speed, even with higher values for C'_{μ_N}, although vastly superior to the original 5 per cent chord nozzle.

In general, these results confirmed the provisional conclusions drawn from the tests on the first leading-edge blowing assembly, particularly as regards the choice of a compromise nozzle position for the aircraft. Reasonable agreement has been obtained between predictions based on tests with a $1\frac{1}{2}$ per cent chord nozzle position and the flight performance of the Buccaneer aircraft (*see* Appendix B). Obviously, since the wing stall commenced on the inboard unblown wing, limited scope remained for further leading-edge development, for instance by extension of the leading-edge blowing nozzle towards the wing root. However, further attention to the outboard wing could well prove necessary, in order to preserve a root stall.

More generally, although a reasonably satisfactory compromise has been achieved for the present application, within the prescribed aircraft design limitations, it is apparent that a fully effective leading-edge blowing arrangement necessitates a carefully-designed nose contour shape to ensure the avoidance of local supercritical free-stream regions under high lift conditions. Particularly with small nose radii, the additional complexity of, say, a leading-edge flap with B.L.C. at the flap knuckle[1,9,10] would seem preferable usually to an integral leading-edge arrangement, so as to allow a more straightforward development process and to avoid compromising the cruise configuration. Further, a more powerful and flexible aerodynamic performance at high lift could be anticipated, particularly as regards the achievement of specified stall and post-stall characteristics.

Some further guidance on possible compressibility effects for high-lift B.L.C. blowing arrangements, and the flow phenomenon involved, may result from comparative sectional tests at R.A.E. on a four-foot chord pressure-plotting model, with alternative normal and high pressure-ratio (up to 9:1) nozzles, initially for leading-edge knuckle and trailing-edge shroud blowing arrangements.

6. *Concluding Remarks.*

Low speed longitudinal stability measurements are described on a half-model of the Blackburn Buccaneer Mark I, with blowing at the integral wing leading edge and shroud blowing over the trailing-edge flap and drooped aileron. Some comparisons with complete-model tests by the firm generally confirm the usefulness of the large-scale half-model for detailed wing development testing.

By the application of shroud blowing over the trailing-edge flap and drooped aileron, the lift increment at constant incidence was nearly doubled. Because of the large spanwise extent of aileron, increases of mean aileron droop angle were particularly beneficial. The presence of shroud blowing permitted mean aileron droop angles as high as 30°, subject to aircraft thrust, yawing moment and rolling moment considerations, with total (flap + drooped aileron) lift increments approaching 1·0, and the preservation of aileron control capability up to the maximum aileron deflection of 45°. Because of the wing sweepback and small tail-arm, the trimming lift losses typically amounted to some 20 per cent of the total lift increment.

The main tests concerned the development and optimisation of a suitable leading-edge blowing arrangement for the Mark I aircraft. For structural reasons, an integral leading edge was specified, although the relatively thin wing (typically 8 per cent R.A.E. 101 with some nose camber) necessitated by cruise drag considerations inevitably led to very high negative pressure peaks and severe adverse pressure gradients under high-lift conditions. The spanwise extent of leading-edge blowing was limited to the main wing,

outboard of the wing fold position.

The minimum aircraft take-off objective, of $C_{L_{max}} \geqslant 1{\cdot}8$ and $\alpha_{stall} \geqslant 20°$, with a limit on aileron mean droop to 20° from engine thrust considerations, was achieved with some difficulty. However, the effectiveness of the leading-edge blowing arrangement was found to depend not only on chordwise position and C_{μ_N}, but also on main-stream Mach number and blowing pressure ratio, because of the proximity to supercritical local free-stream velocities at representative main-stream speeds. A safe compromise was chosen for the aircraft, with some loss of effectiveness. The chosen leading-edge arrangement ensured a root stall, with some delay before the spread of the stall to the remainder of the wing, and only moderate post-stall reductions in lift, even at extreme aileron deflections. However, pitch-up at the stall was not avoided and good post-stall characteristics could not be ensured with the prescribed integral leading edge.

The Buccaneer Mark I aircraft shows flight performance under high-lift conditions which is in good general agreement with the model tests with the aircraft leading-edge nozzle position. Since the onset of wing stall is determined by flow separations on the unblown inboard wing, there is some scope for further development, for instance by extension of the spanwise extent of the leading-edge blowing nozzle. However, to preserve the present root stall, without increasing the rate of spread of the initial flow separations, further attention to the outboard wing nose may also prove necessary.

In similar applications to high-speed thin-wing aircraft, the additional mechanical complexity of a leading-edge flap with B.L.C. would seem preferable to the present integral leading-edge arrangement, to avoid compromising the cruise configuration and to allow more straightforward development. The problems of optimising the nozzle position would be much reduced as also would the flow requirements, especially if adverse compressibility effects were thus avoided. Equally important, a more powerful and flexible aerodynamic performance could be expected, particularly as regards the achievement of specified stall and post-stall characteristics.

Some further guidance on compressibility effects for high-lift B.L.C. arrangements should result from comparative sectional tests at R.A.E. on a four-foot chord pressure-plotting model, with alternative normal and high-pressure ratio nozzles (up to 9:1), initially for leading-edge knuckle and trailing-edge shroud blowing configurations.

Acknowledgements.

H.S.A. (Brough) constructed the model and assisted with the testing and analysis of results, as well as providing data for the tunnel and flight comparisons presented in the Appendices.

LIST OF SYMBOLS

A	Wing aspect ratio
b	Total wing span
c	Local wing chord
$\bar{c}$	Standard mean chord
$\bar{\bar{c}}$	Aerodynamic mean chord
C_D	Total drag coefficient including jet thrust
ΔC_D	Drag coefficient increment at constant C_L
ΔC_{D_c}	Tunnel constraint correction to drag coefficient
$C_L, C_{L_{max}}, \bar{C}_L$	Lift coefficient, maximum lift coefficient, trimmed lift coefficient
ΔC_L	Lift coefficient increment at constant α_w
ΔC_{L_t}	Lift coefficient increment due to trimming
C_m	Pitching-moment coefficient, based on $\bar{c}$, referred to 0·25 $\bar{c}$
ΔC_m	Pitching-moment coefficient increment at constant C_L
ΔC_{m_c}	Pitching-moment coefficient tunnel constraint correction (tailplane-on runs)
ΔC_{m_t}	Pitching-moment coefficient increment due to tailplane
C_{μ_N}, C_{μ_R}	$\frac{(m\,v_J)_N}{\frac{1}{2}\rho_0 U_0^2 Sg}, \frac{(m\,v_J)_R}{\frac{1}{2}\rho_0 U_0^2 Sg}$; blowing momentum coefficients based on gross wing area, for nose and rear nozzles
$C'_{\mu_N}, C'_{\mu R}$	$C_{\mu_N}\frac{S}{S'_N}, C_{\mu_R}\frac{S}{S'_R}$; average sectional blowing momentum coefficients based on blown wing area S'_N, S'_R for nose and rear nozzles
C_p	Surface static pressure coefficient
C_p^*	Critical value of C_p for sonic conditions at main-stream Mach number M
g	Acceleration due to gravity
m	Measured mass flow rate of blowing air
M	Mainstream Mach number
p_D	Mean total pressure of blowing air
S	Gross area of half wing
S'_N	Wing area spanned by blowing nozzle at wing nose
S'_R	Wing area spanned by blowing nozzle at wing shroud
S_t	Gross area of half tailplane
V_0	Mainstream speed
v_J	Mean jet velocity after expansion to free-stream static pressure
α_w	Wing incidence

LIST OF SYMBOLS—*continued*

α_s	Wing maximum lift incidence
ε	Mean downwash angle at tailplane
η_t	Tailplane setting relative to fuselage datum
ξ	Mean droop of aileron
ρ_0	Main-stream density
$\frac{1}{2}\rho_0 U_0^2$	Main-stream dynamic head
$\frac{dC_m}{d\eta_T}$	Tailplane power

REFERENCES

No.	*Author(s)*	*Title, etc.*
1	J. Williams and S. F. J. Butler . .	Aerodynamic aspects of boundary-layer control for high lift at low speeds. *Journ. Roy. Ae. Soc.*, Vol. 67, pp 201–223 (1963). AGARD Report No. 414 (1963).
2	S. F. J. Butler and M. B. Guyett	Low-speed wind-tunnel tests on the de Havilland Sea Venom with blowing over the flaps. A.R.C. R. & M. 3129 (1957).
3	S. F. J. Butler and M. B. Guyett	Low-speed wind-tunnel tests on a delta-wing aircraft model (S.R. 177) with blowing over the trailing-edge flaps and ailerons. A.R.C. C.P. 710 (1962).
4	A. Anscombe, S. F. J. Butler . . and M. B. Guyett	Low-speed wind-tunnel tests on the Vickers-Supermarine N.113 (Scimitar) with blowing over the trailing-edge flaps. R.A.E. Technical Note 2905 (1963). A.R.C. 25417.
5	A. Anscombe and J. Williams . .	Some comments on high-lift testing in wind tunnels with particular reference to jet-blowing models. AGARD Report No. 63 (1956). R.A.E. Technical Note Aero 2460 (1956). A.R.C. 18664.
6	S. F. J. Butler and J. Williams . .	Further comments on high-lift testing in wind tunnels with particular reference to jet-blowing models. R.A.E. Technical Note Aero 2632 (1959). A.R.C. 21690. *Aero Quart.* Vol. XI, pp 285–308 (1960). AGARD Report No. 304 (1959).
7	E. C. Maskell	A theory of the blockage effects on bluff bodies and stalled wings in a closed wind tunnel. A.R.C. R. & M. 3400 (1963).
8	A. F. Jones and W. R. Buckingham	Some exploratory tests on a two-dimensional blown-cylinder model in the R.A.E. 2ft × 1½ft transonic wind tunnel. R.A.E. Technical Report 64090 (A.R.C. 26850) (1964).
9	S. F. J. Butler and J. Lawford . .	Low-speed wind-tunnel tests on a wing-fuselage model with area suction through perforations at the leading-edge flap knee. R.A.E. Technical Report 67153 (1967).
10	R. C. W. Eyre and S. F. J. Butler	Low-speed wind-tunnel tests on an AR8 swept wing subsonic transport research model with B.L.C. blowing over nose and rear flaps for high lift. R.A.E. Technical Report 67112 (1967). A.R.C. 29389.
11	A. M. H. Dunn	Blowing the Buccaneer. *Flight International*, pp 754–756 (1966).

APPENDIX A

Comparison of Half-Model and Complete-Model Test Results.

During the initial tests on the 1/5-scale half-model in the H.S.A. (Brough) 7ft × 5ft wind tunnel, the fuselage had to be foreshortened and the validity of tunnel constraint and blockage estimates $\left(\frac{S}{C} = 0{\cdot}34\right)$ is open to question particularly near to the stall. However, comparisons can usefully be attempted between the present tests on this model in the R.A.E. $11\frac{1}{2}$ft × $8\frac{1}{2}$ft tunnel and on a 1/12-scale complete model in the H.S.A. 7ft × 5ft tunnel. Fortunately, the estimated lift constraint and blockage corrections are virtually identical for the two cases and of acceptable magnitude (e.g. $\Delta\alpha = 1{\cdot}65°$ at $C_L = 2$).

Close agreement is achieved between the corresponding C_L *vs.* α_w curves below the stall (Fig. 27), confirming the validity of the half-model technique and the general compatability of the test procedures adopted in the two facilities, for instance, as regards measurement of C_μ-values. However, the small scale of the complete model and the limited R.N. (about $1{\cdot}25 \times 10^6$) combined to preclude the achievement of representative stall development, without or with leading-edge blowing.

Drag and pitching-moment comparisons indicate reduced pitching-moment increments and lower values of $\frac{dC_D}{dC_L^2}$ and C_{D_0} for the complete model. On the other hand, surprisingly good agreement in variations of mean downwash at the tailplane is achieved (*see* Fig. 10) despite the partial immersion of the half-tailplane in the tunnel floor boundary layer.

The half-model technique can usefully be applied for detailed high-lift wing development, particularly where the use of a complete model would necessitate an inadequate model scale or R.N. Naturally, a complete model of adequate scale would be preferable to the half-model, partly to minimise the uncertainties introduced by use of a half-model technique, but more to allow wider aerodynamic investigations (e.g. aileron power, lateral stability, super stall, ground effect). In the present instance, a 1/5-scale complete model would be feasible with a wind tunnel having a cross-sectional area of order 200 sq feet (e.g. H.S.A. 15ft × 15ft VSTOL tunnel).

APPENDIX B

Comparison of Model and Aircraft Test Results.

With the appropriate corrections applied, the present results agree well with further aircraft development tests on the same model in the new H.S.A. (Hatfield) 15ft × 15ft tunnel. In order to make valid flight-tunnel comparisons, the H.S.A. programme included tests with certain specific features of the flight test aircraft. With due allowance for the variation of C_μ with α_w for the aircraft, excellent agreement was achieved by H.S.A. for the lift-incidence curve (Fig. 28). This agreement persisted at wing incidences of the order of 18°, representing the limiting usable C_L for this aircraft and close to the model stalling incidence. In the absence of stall tests for the aircraft actual comparisons of $C_{L_{max}}$ and stalling incidence are not possible.

The further comparison of tailplane trim settings for two *cg* positions (Fig. 29) again confirms the degree of agreement between tunnel and flight results, within the limits set by experimental accuracy.

Flight tests have generally confirmed that blowing B.L.C. was as effective as expected[11] allowing for limitations on spanwise continuity of efflux arising from engineering considerations related to control support gear. In particular, the drooped ailerons remained relatively effective at high incidences, enabling incipient wing drop to be corrected.

TABLE 1

Model Data.

All dimensions model scale (i.e. 1/5 of full-scale)

Wing (port half-wing only)	
Area S	10·17 sq ft
Semi-span $\frac{b}{2}$	4·25 ft
Standard rear chord $\bar{c}$	2·395 ft
Aerodynamic mean chord $\bar{\bar{c}}$	2·532 ft
Centreline chord	3·562 ft
Tip chord	1·600 ft
Aspect ratio (based on complete aircraft)	3·55
Taper ratio	0·59
Quarter-chord sweepback (outboard of chord)	30·2°
Quarter-chord sweepback (inboard of chord)	38·6°
Trailing-edge sweepback	20·0°
Basic wing sections	
At aircraft centreline	R.A.E. 100, 9·25%, symmetrical
At 55% semi-span	R.A.E. 101, 8%, cambered
At tip	R.A.E. 102, 8%, cambered
Dihedral	0°
Twist	0°
Wing-fuselage angle	2·5°
Leading-edge flap	
Flap chord	0·15 c outboard of wing blend, increasing inboard of blend
Spanwise extent	$0{\cdot}32\frac{b}{2}$ to $1{\cdot}00\frac{b}{2}$
Flap setting:	27° (along stream) 30° (normal to hinge-line)
Leading-edge slat	
Mean extension	0·15 c
Angular setting	15° (along stream)
Spanwise extent	$0{\cdot}55\frac{b}{2}$ to $1{\cdot}00\frac{b}{2}$
Original leading-edge blowing arrangement	
Spanwise extent	$0{\cdot}47\frac{b}{2}$ to $1{\cdot}00\frac{b}{2}$
Nozzle depth	varying from 0·022 inch at inboard limit to 0·019 inch at outboard limit
Blockage due to spacers	7·4%
Nozzle positions	0·25, 1·5, 2·0 and 5·0% chord

TABLE 1—*continued*

Final leading-edge blowing arrangement	
Spanwise extent	$0{\cdot}51\frac{b}{2}$ to $1{\cdot}00\frac{b}{2}$
Nozzle depth	varying from 0·018 inch at inboard limit to 0·011 inch at outboard limit
Blockage due to spacers	Nil
Nozzle positions	0·25, 1·5% chord
Blown wing area S'_N	4·10 sq ft
S/S'_N	2·60
Trailing-edge flap	
Flap chord (aft of hinge-line)	0·223 c (mean)
Sweepback of hinge-line	23·4°
Spanwise extent	$0{\cdot}26\frac{b}{2}$ to $0{\cdot}44\frac{b}{2}$
Flap settings:	28°, 42½°, 58°, 73½° (alongwind) 30°, 45°, 60°, 75° (normal to hinge-line)
Trailing-edge aileron	
Aileron chord (aft of hinge-line)	0·244 c (outboard of blend)
Sweepback of hinge-line	23·4°
Spanwise extent	$0{\cdot}44\frac{b}{2}$ to $1{\cdot}00\frac{b}{2}$
Aileron settings:	12°, 18½°, 28°, 42½° (alongwind) 13°, 20°, 30°, 45° (normal to hinge-line)
Shroud blowing arrangement	
Spanwise extent	$0{\cdot}26\frac{b}{2}$ to $1{\cdot}00\frac{b}{2}$
Nozzle depth	varying from 0·028 inch at inboard limit to 0·016 inch at outboard limit
Blockage due to spacers	4·3%
Blown wing area, S'_R	6·54 sq ft
S/S'_R	1·55
Tailplane (port half-tailplane only)	
Area, S_t	1·510 sq ft
Semi-span, $\frac{b_t}{2}$	1·426 ft
Standard mean chord	1·06 ft
Aspect ratio (based on complete tailplane)	2·69
Tail arm (cg to mean quarter-chord point)	4·69 ft
Height of tailplane above fuselage datum	1·80 ft
Sweepback of quarter-chord line	25°
Dihedral	0°
Taper ratio	0·58
Basic section	R.A.E. 102, 5%, with negative camber

TABLE 1—*continued*

Tailplane flap

Flap chord	0·32 c (mean)
Sweepback of hinge-line	17°
Spanwise extent	$0{\cdot}06\frac{b_t}{2}$ to $1{\cdot}00\frac{b_t}{2}$
Flap setting:	29° up (alongstream) 30° up (normal to hinge-line)

Fuselage

Basic Buccaneer Mark I fuselage, without nose extension
Natural airflow through engine nacelle

Test cg

On wing chord plane and fuselage datum, at 0·25 $\bar{c}$, 2·32 ft aft of projected wing leading-edge apex and 5·52 ft aft of fuselage nose

Test Reynolds numbers

Based on wing standard mean chord:
$2{\cdot}1 \times 10^6$ at 140 ft/sec
$3{\cdot}0 \times 10^6$ at 200 ft/sec

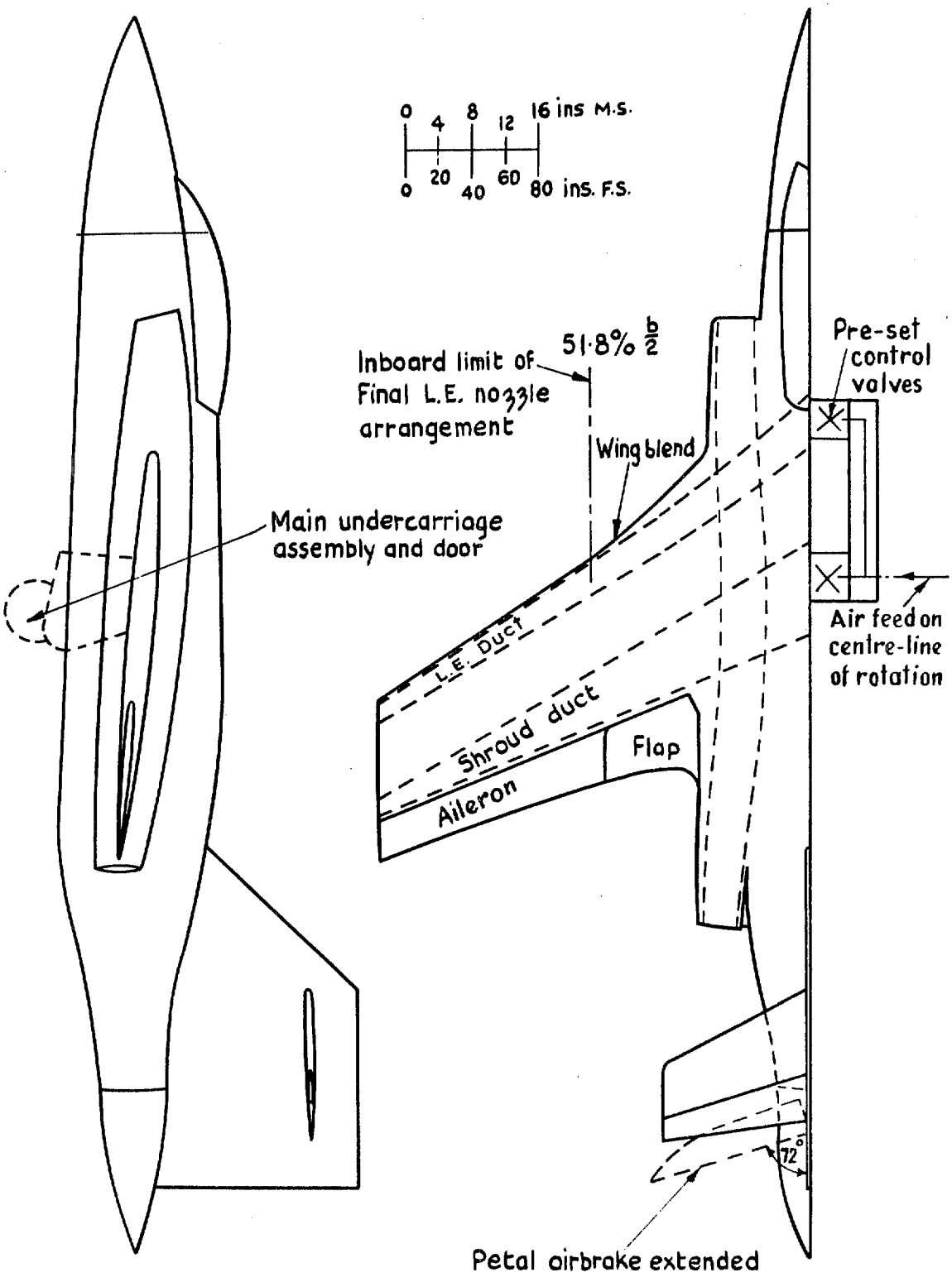

FIG. 1. G.A. of model.

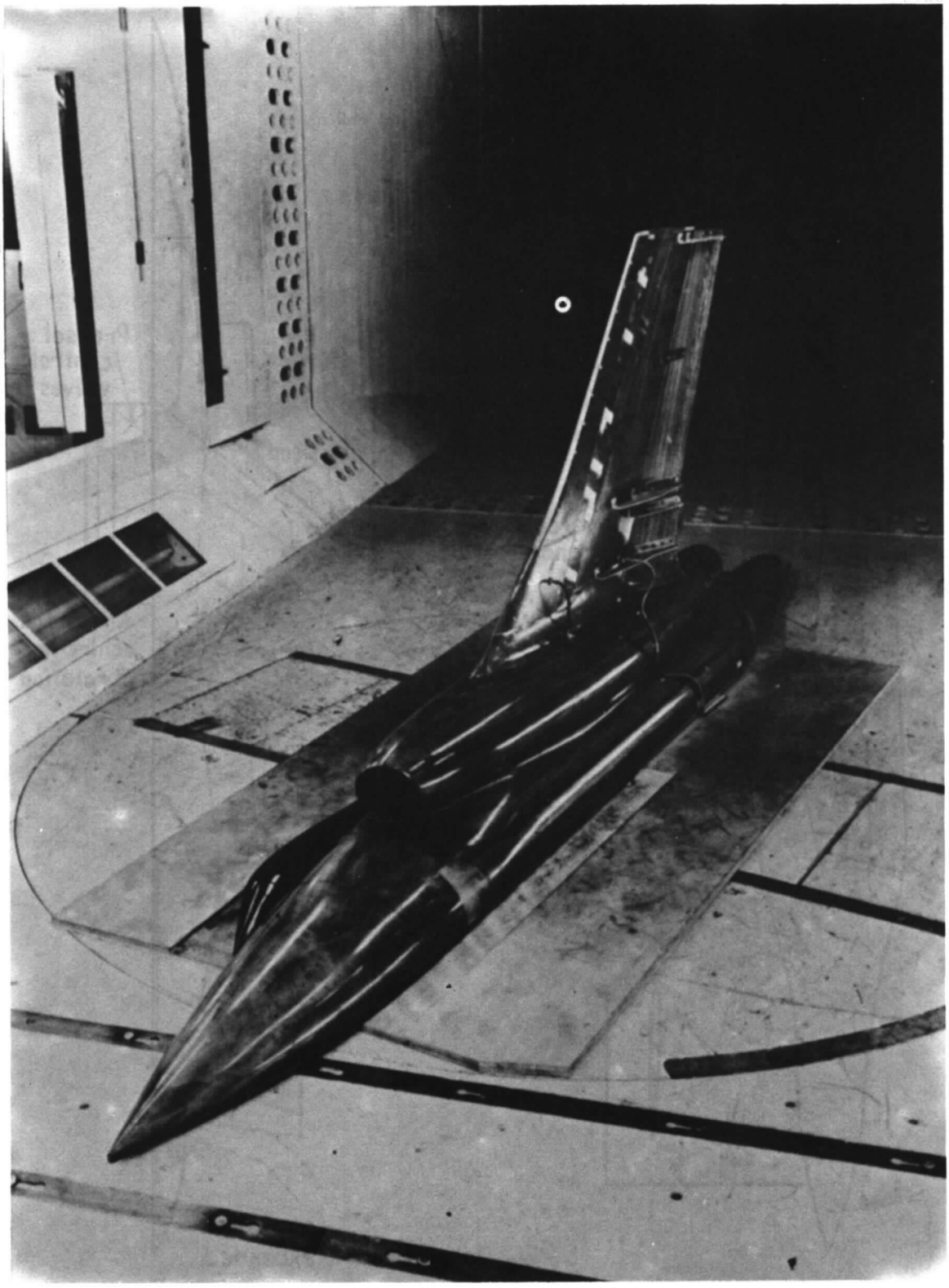

FIG. 2. Buccaneer Mk. I half-model in R.A.E. No. 2 $11\frac{1}{2}$ft × $8\frac{1}{2}$ft wind tunnel.

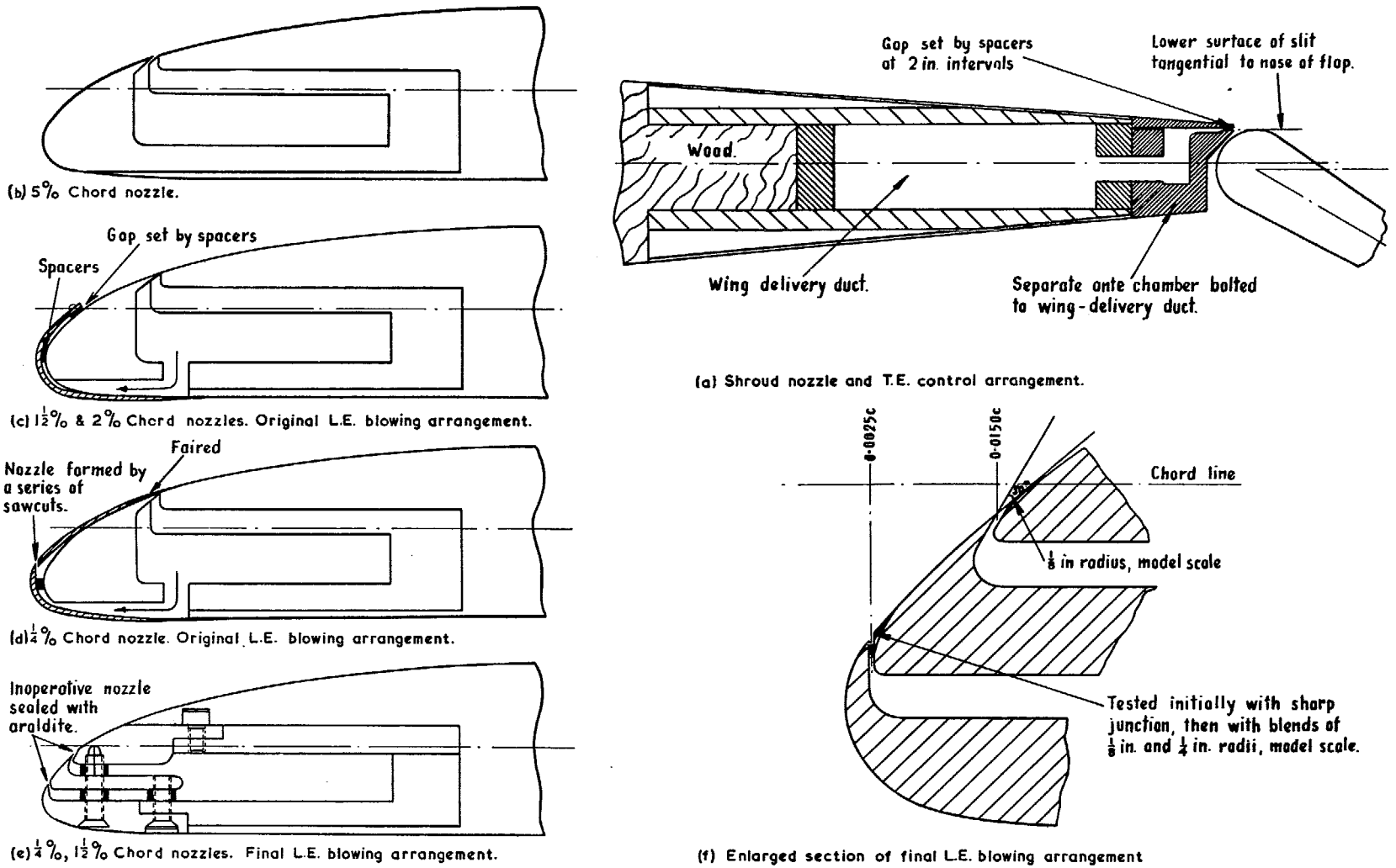

FIG. 3. Details of L.E. and T.E. blowing nozzles.

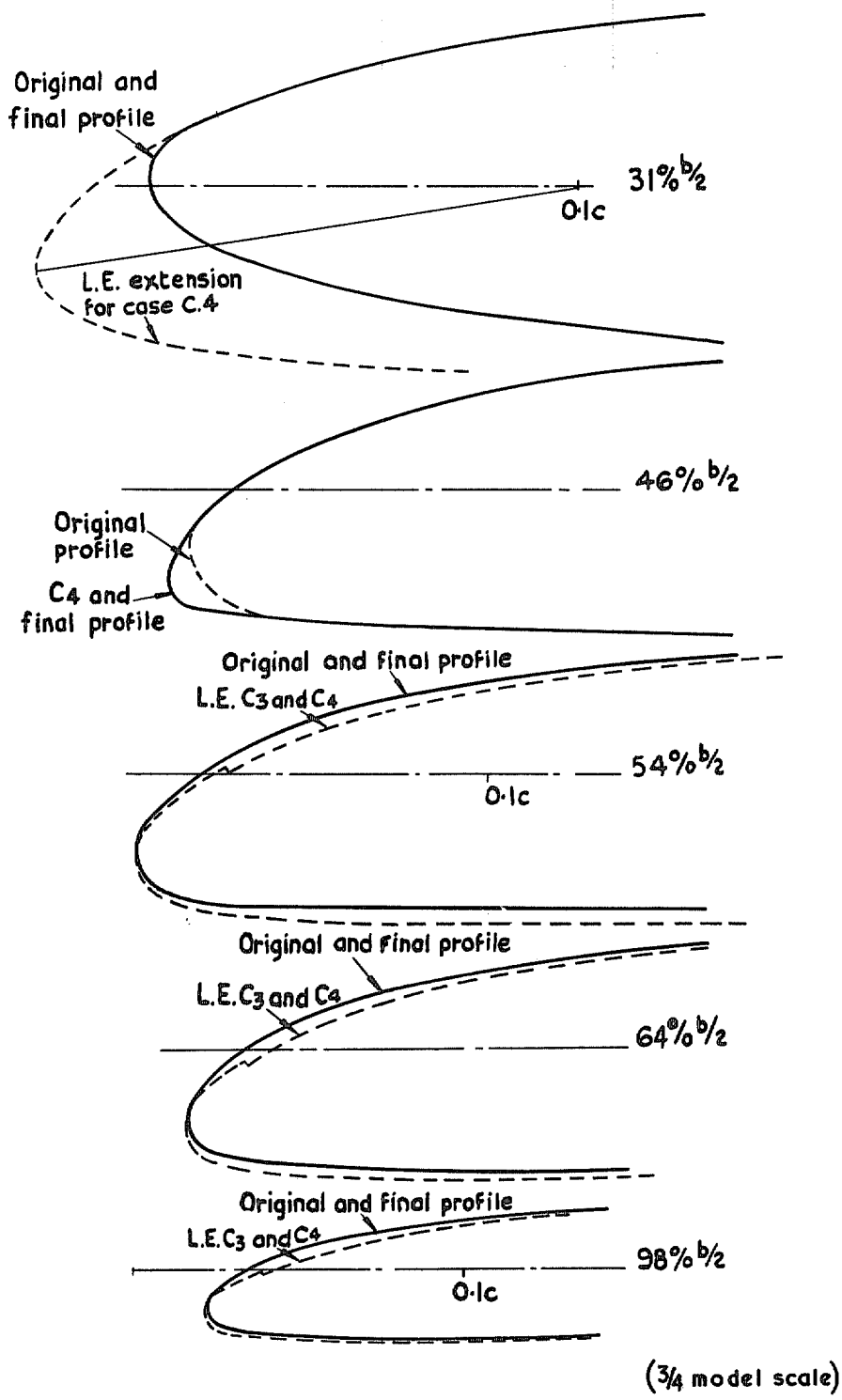

FIG. 4. Details of L.E. profiles.

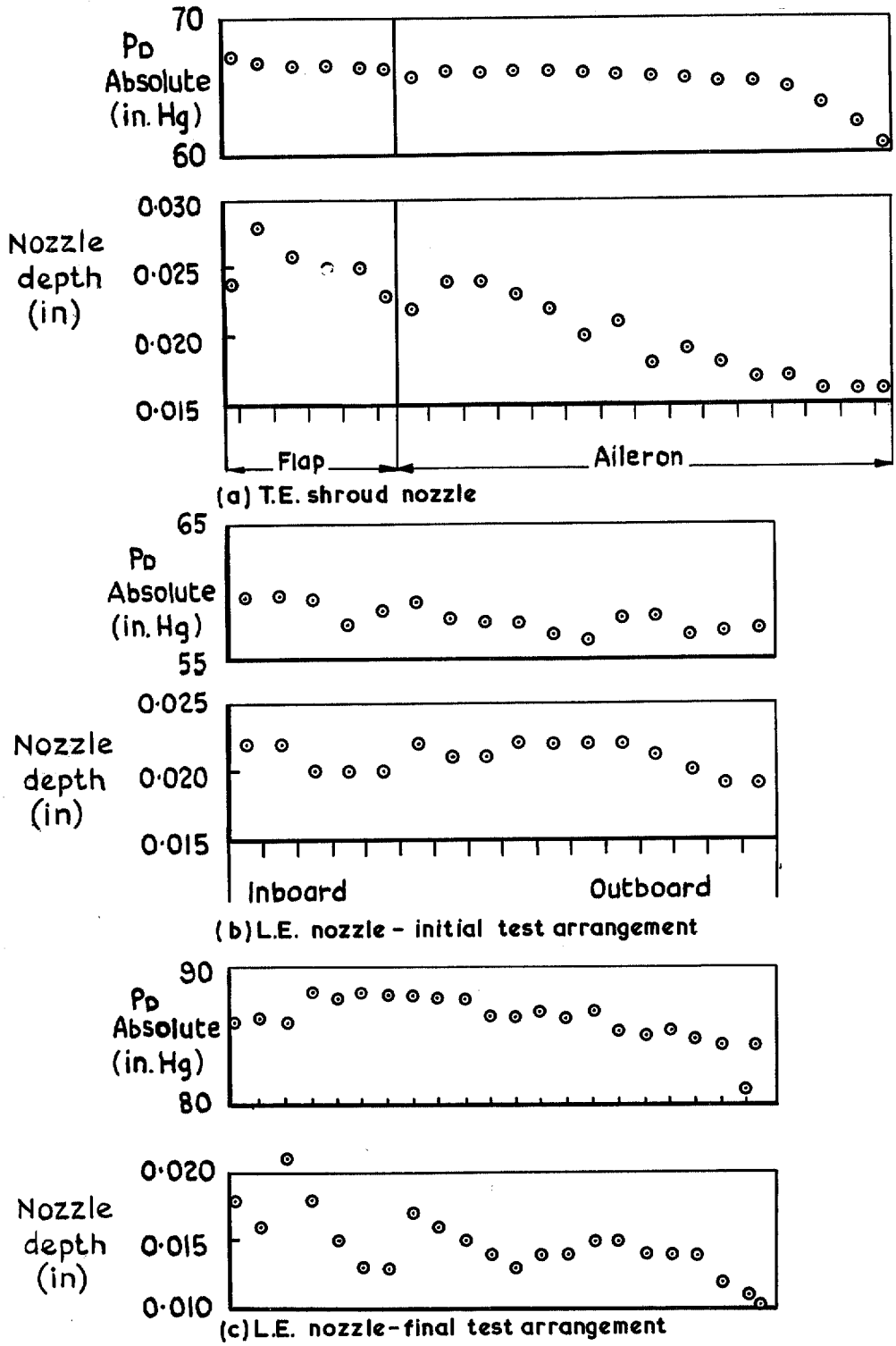

FIG. 5. Spanwise distributions of total head and nozzle depth.

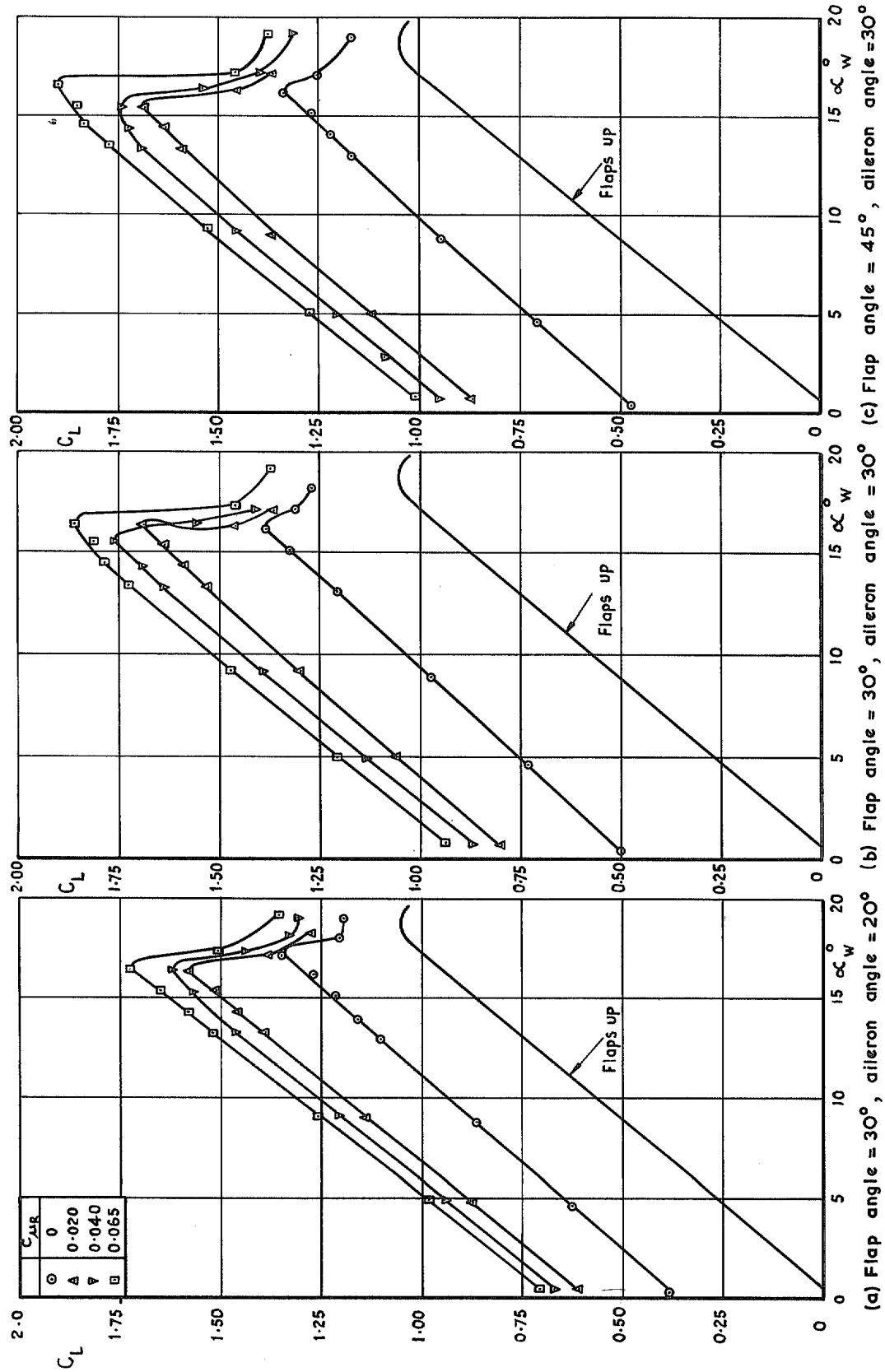

FIG. 6. The effect of shroud blowing over flap and aileron on C_L (no tailplane) *vs.* α_w. Standard L.E., without L.E. blowing.

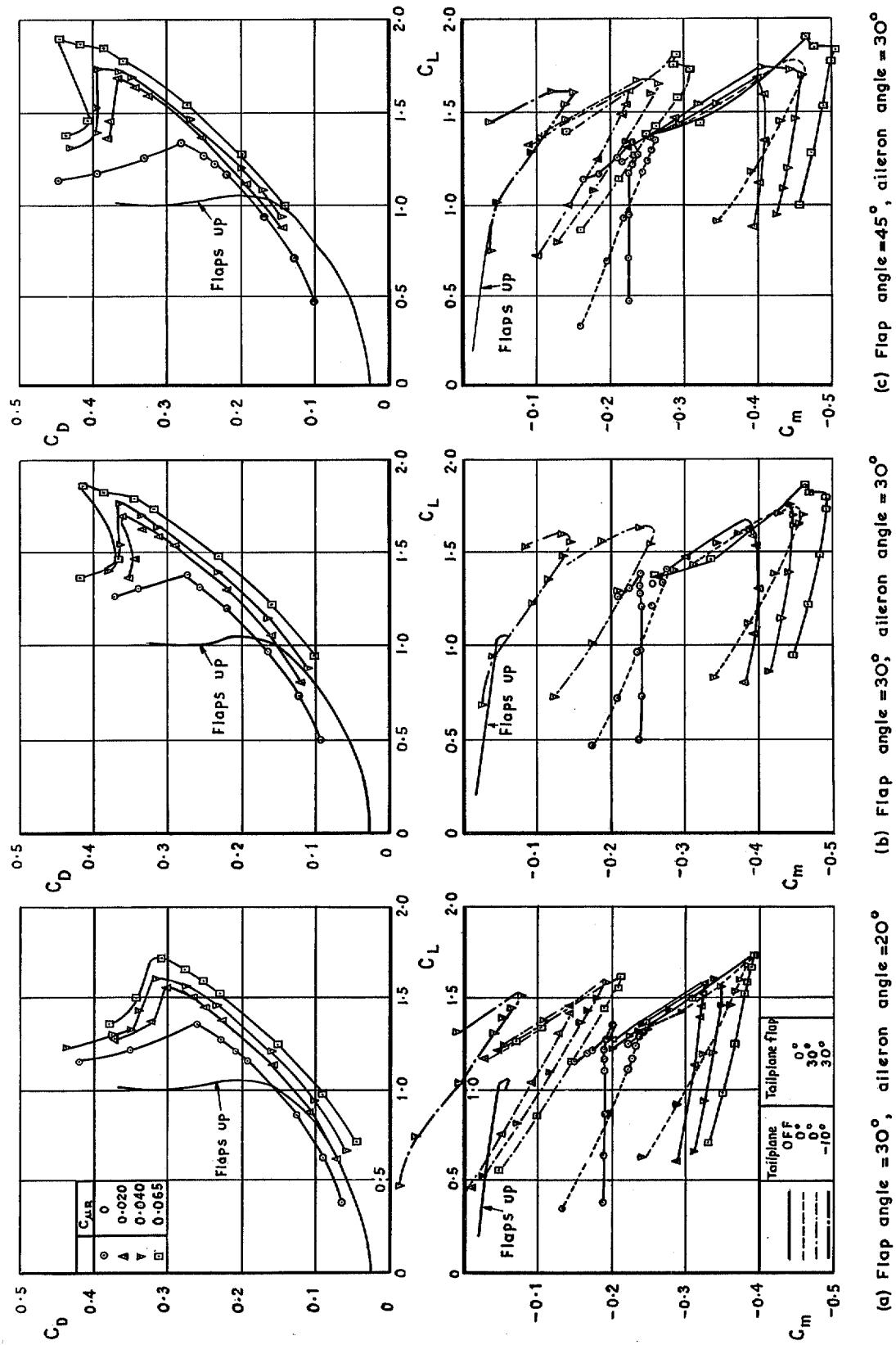

FIG. 7. The effect of shroud blowing over flap and aileron on C_D *vs* C_L (no tailplane) and C_m *vs* C_L. Standard L.E., without L.E. blowing.

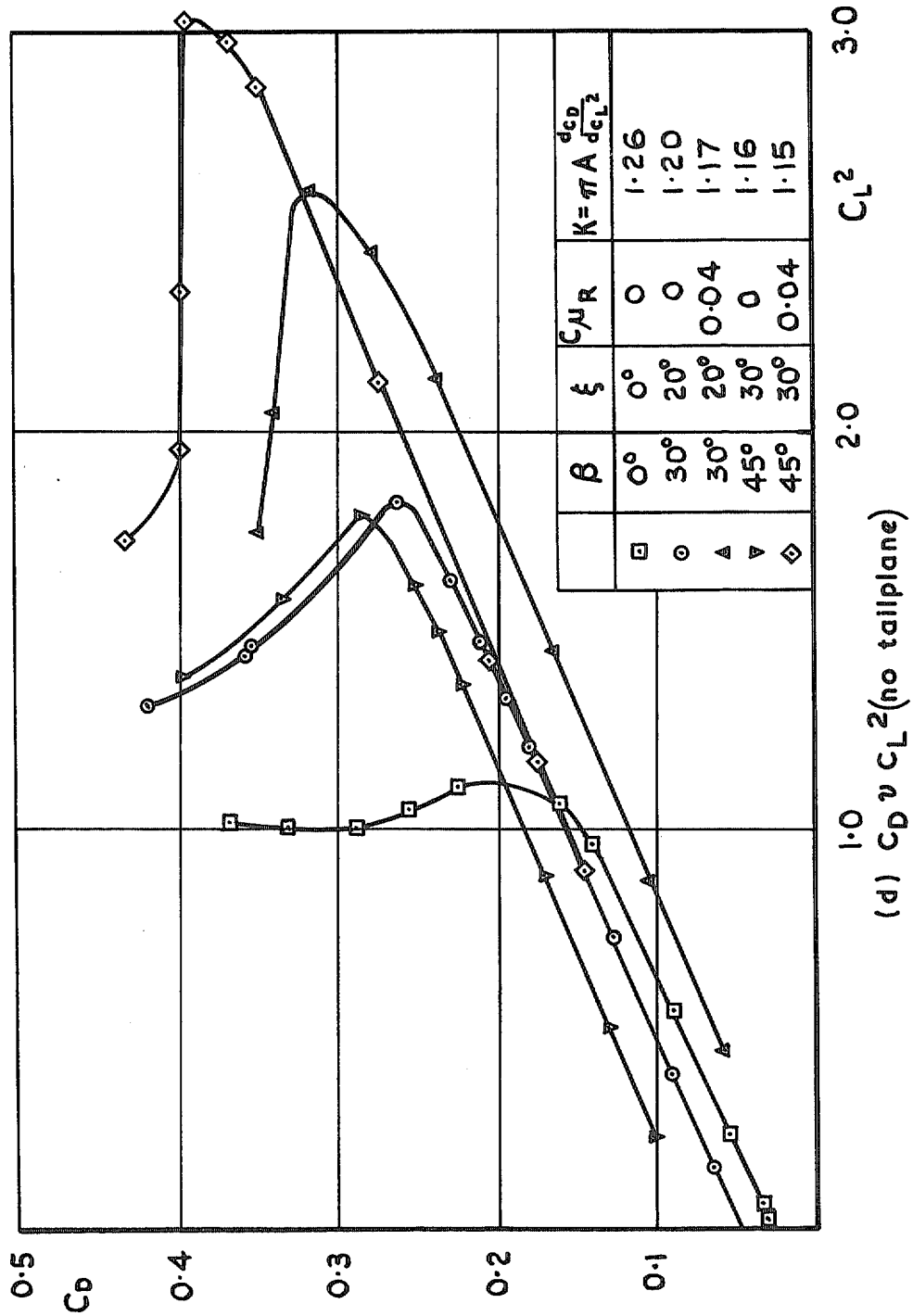
(d) C_D v C_L^2 (no tailplane)
C_D
C_L^2
0·5
0·4
0·3
0·2
0·1
1·0
2·0
3·0
β
ξ
$C\mu_R$
$K = \pi A \frac{d c_D}{d c_L^2}$
0° 0° 0 1·26
30° 20° 0 1·20
30° 20° 0·04 1·17
45° 30° 0 1·16
45° 30° 0·04 1·15

FIG. 7 (*contd.*).

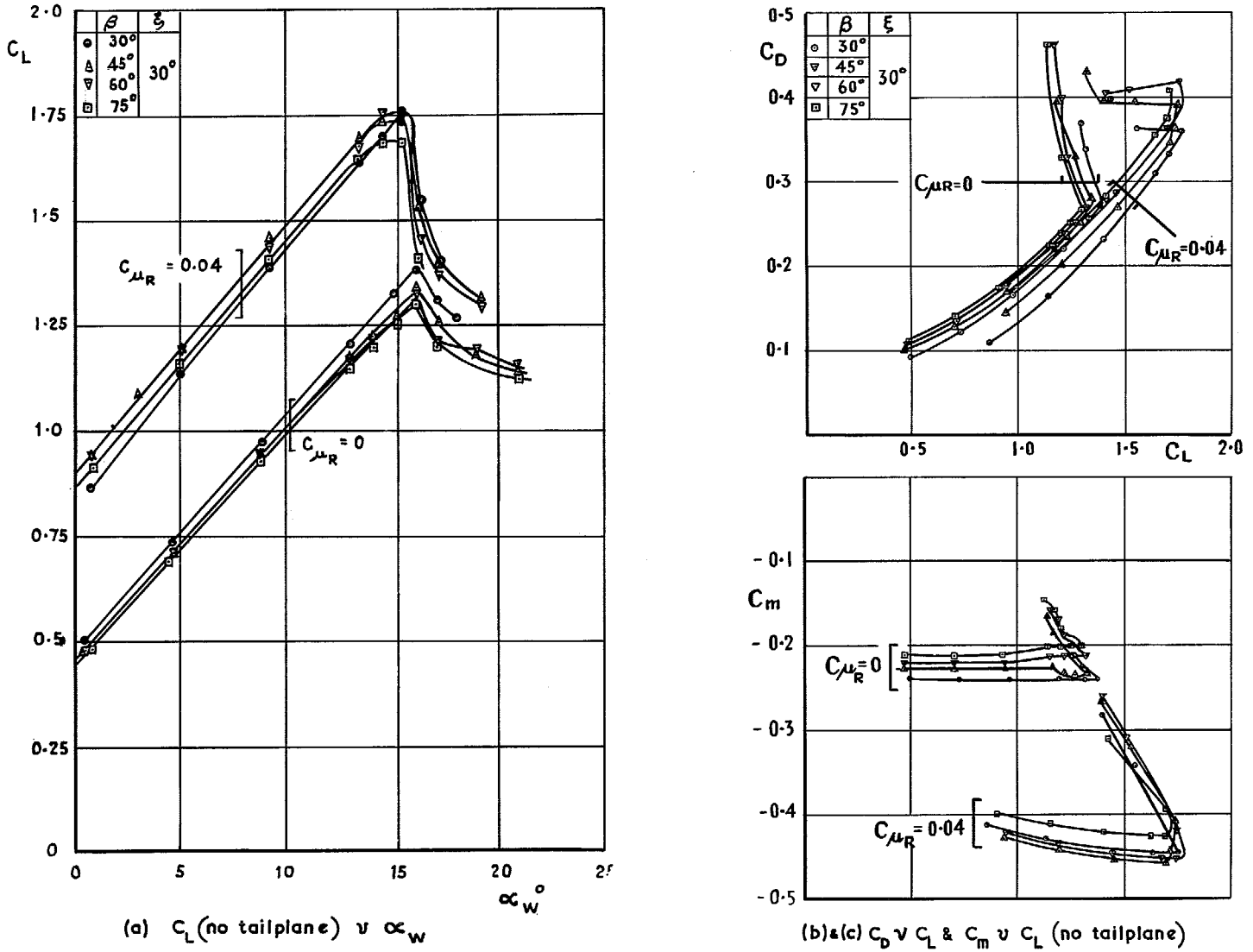

FIG. 8. The effect of T.E. flap angle. Standard L.E., without L.E. blowing.

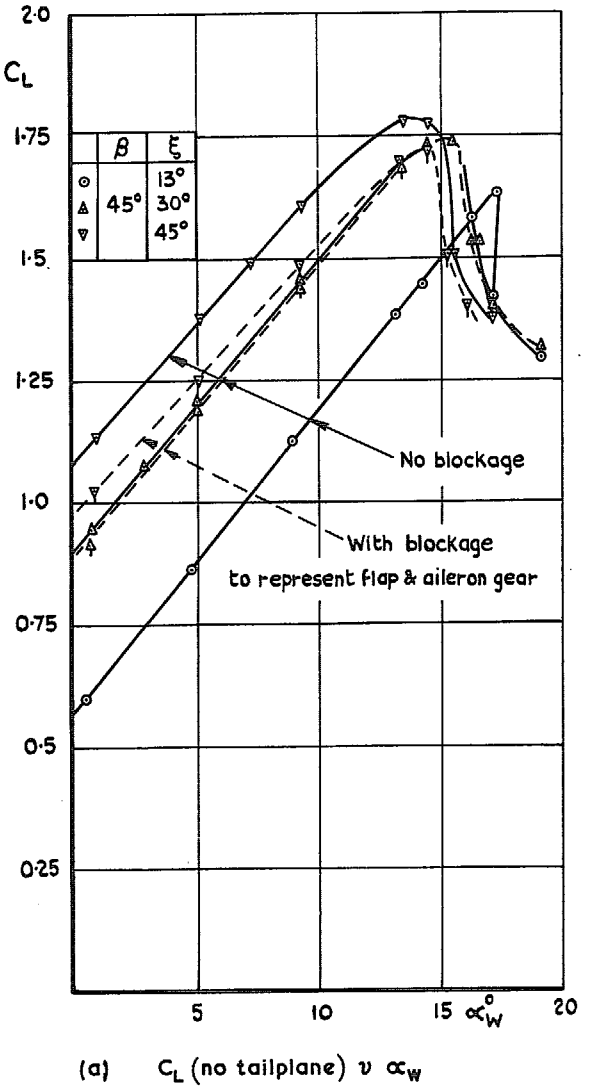

(a) C_L (no tailplane) v α_W

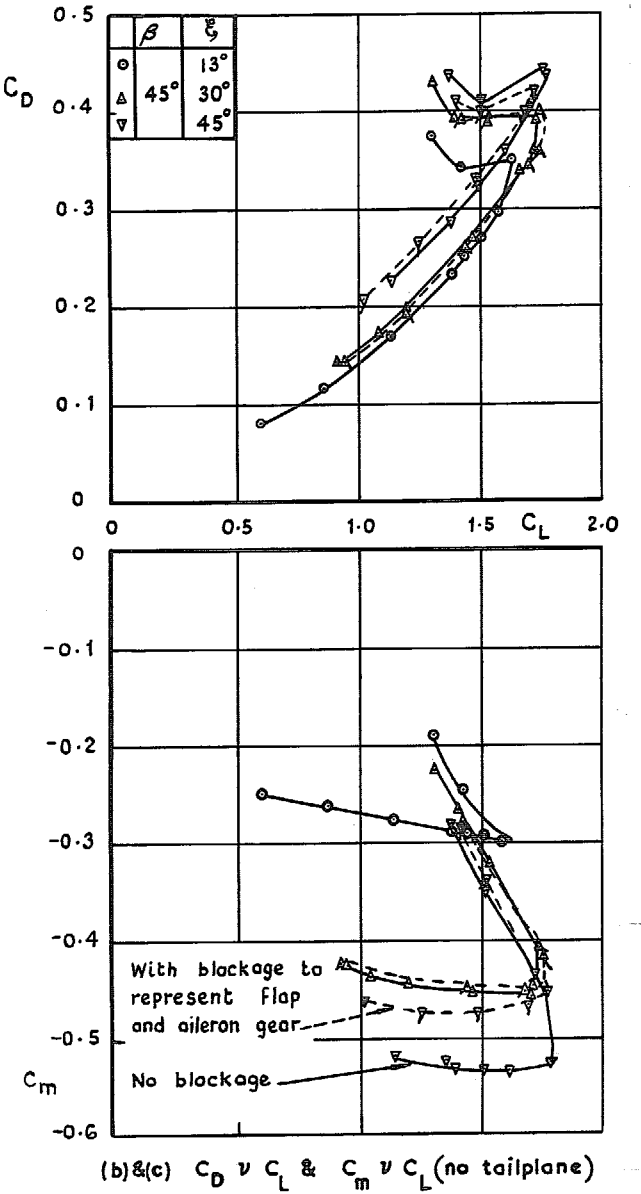

(b)&(c) C_D v C_L & C_m v C_L (no tailplane)

FIG. 9. The effect of partial blockage of T.E. shroud blowing nozzle. Standard L.E., without L.E. blowing $C_{\mu_R} = 0{\cdot}04$.

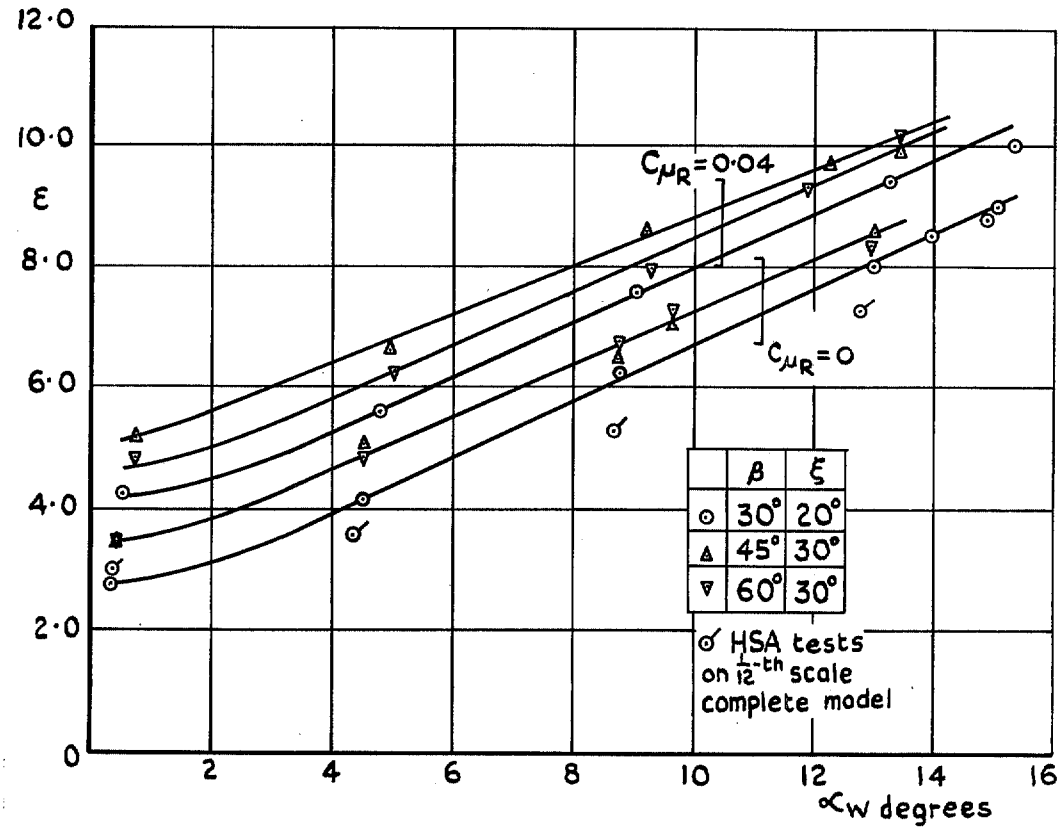

FIG. 10. Downwash at the tailplane.

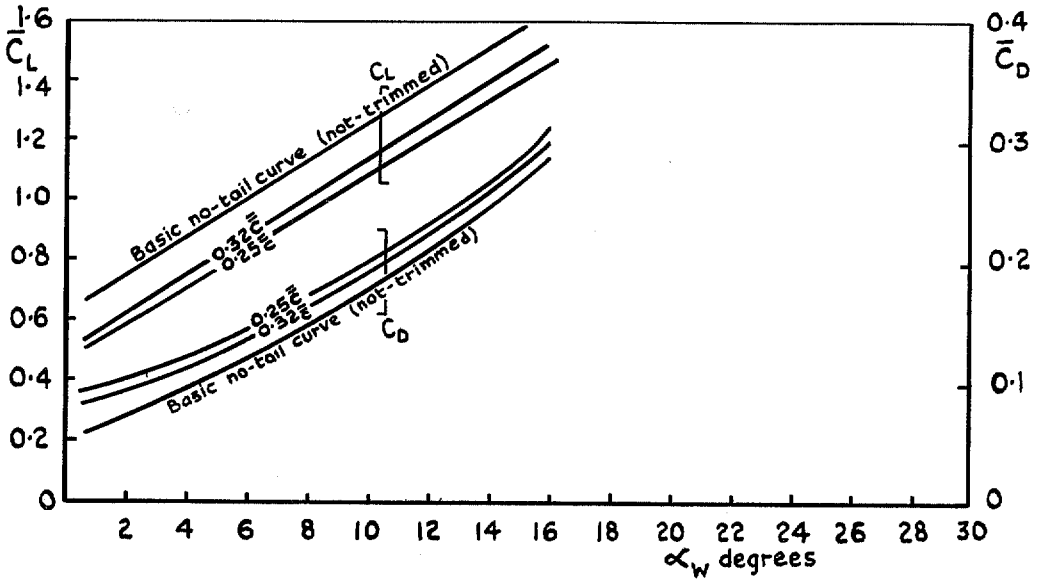

FIG. 11. The effect of trimming on C_L *vs* α_w and C_D *vs* α_w. $\beta = 30°$, $\xi = 20°$, $C_{\mu_R} = 0{\cdot}04$.

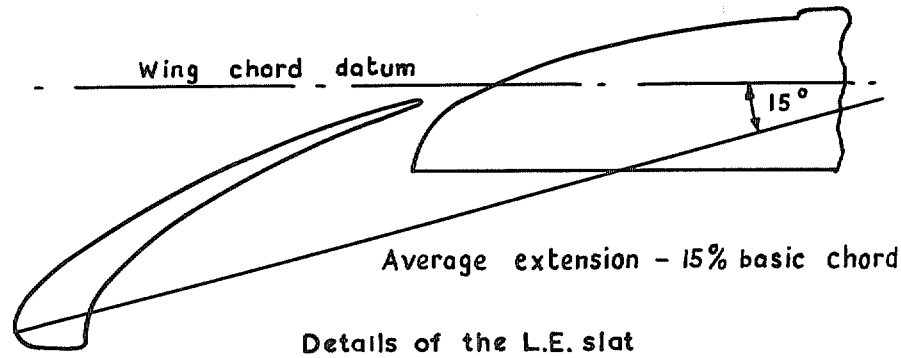

Details of the L.E. slat

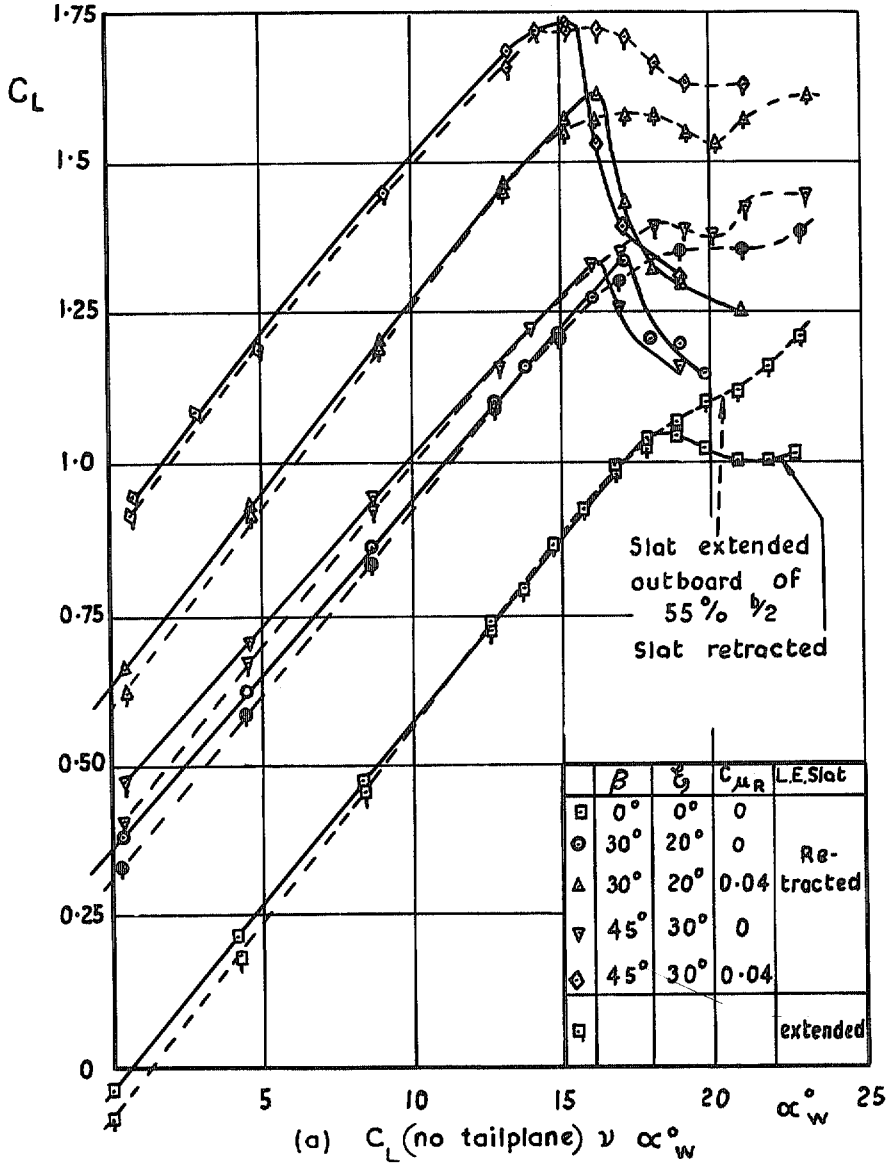

FIG. 12. The effect of the L.E. slat.

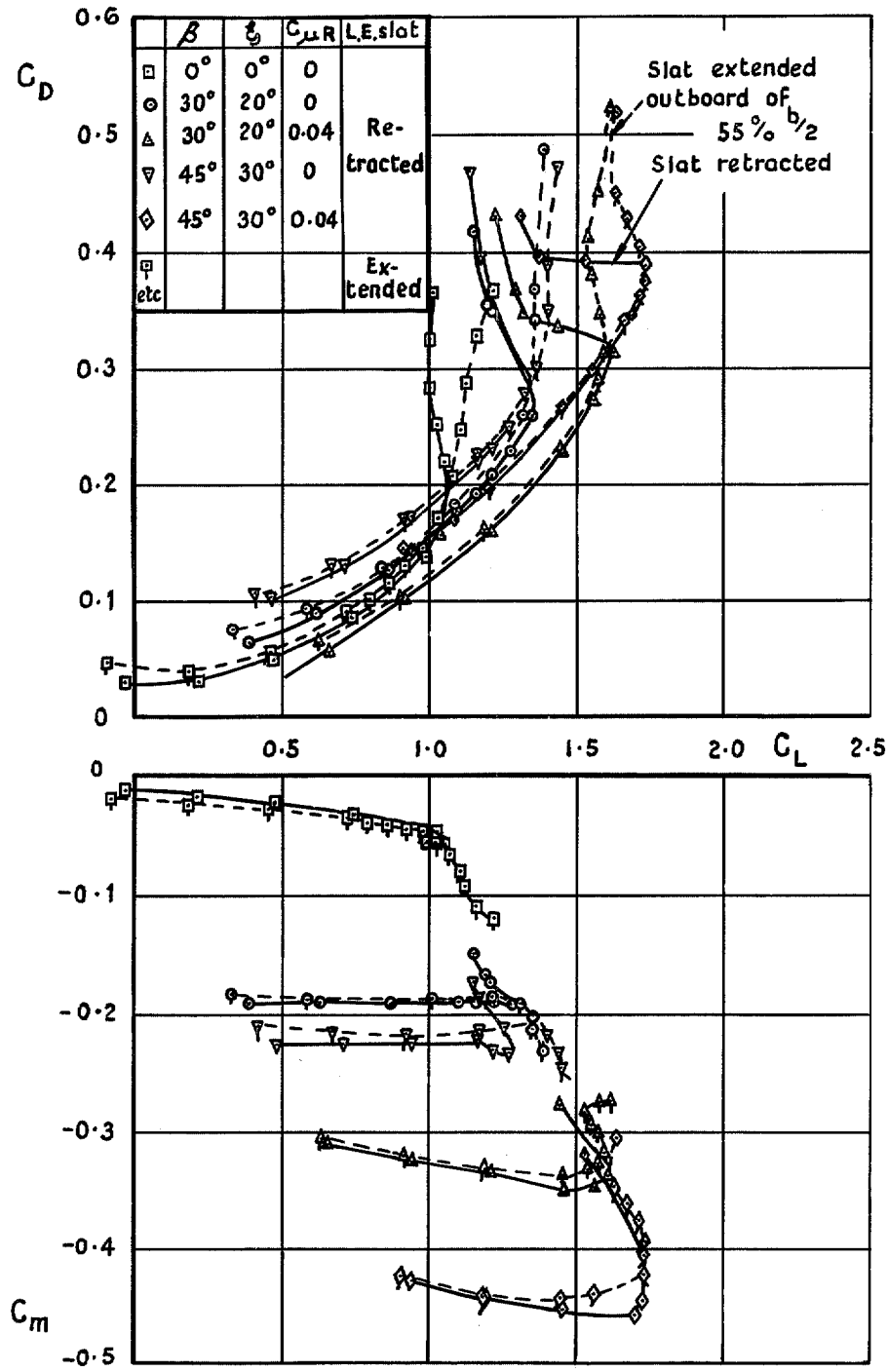

(b) & (c) C_D v C_L & C_m v C_L (no tailplane)

FIG. 12 (*contd.*).

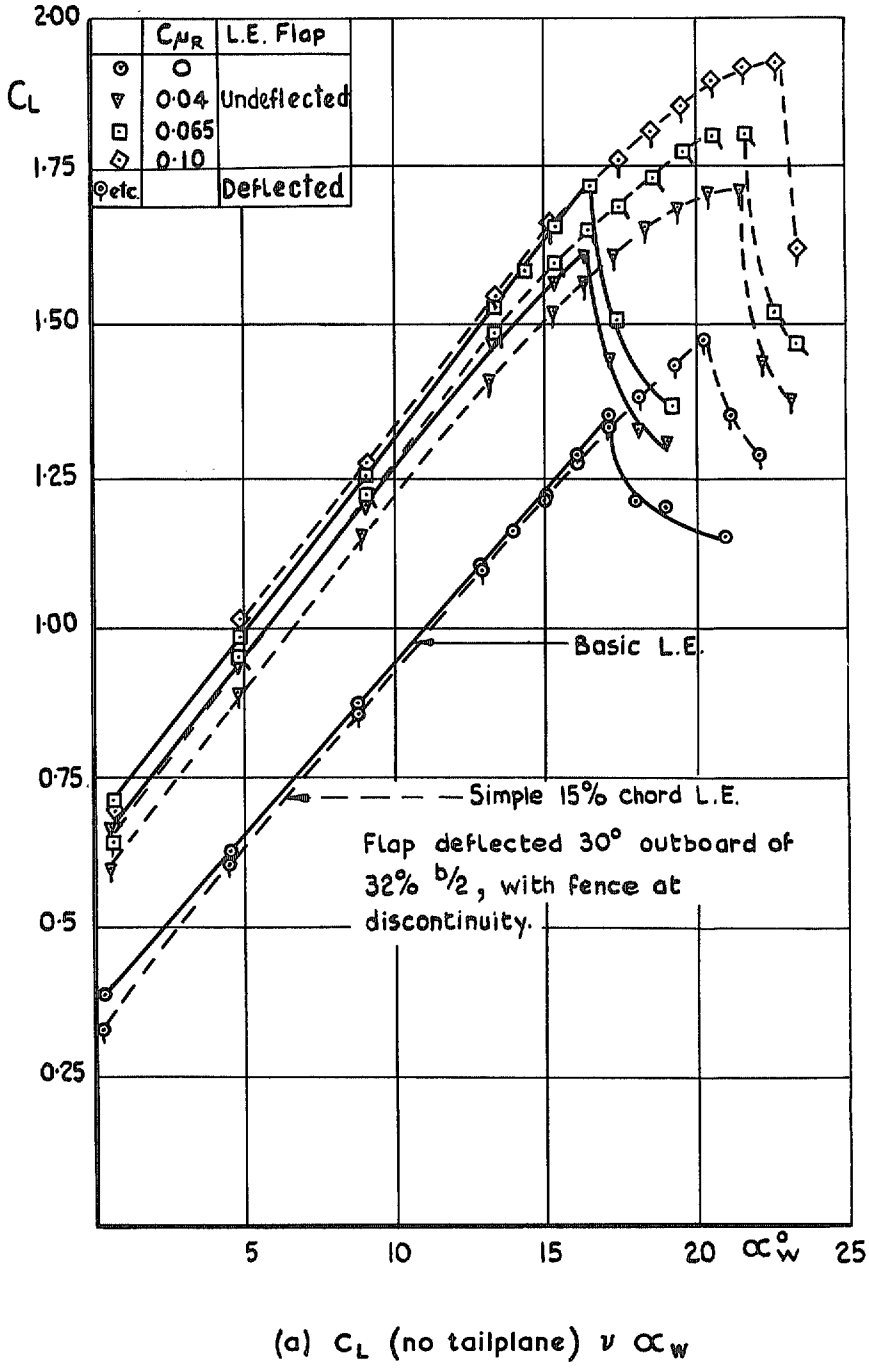

FIG. 13. The effect of the L.E. flap. $\beta = 30°$, $\xi = 20°$.

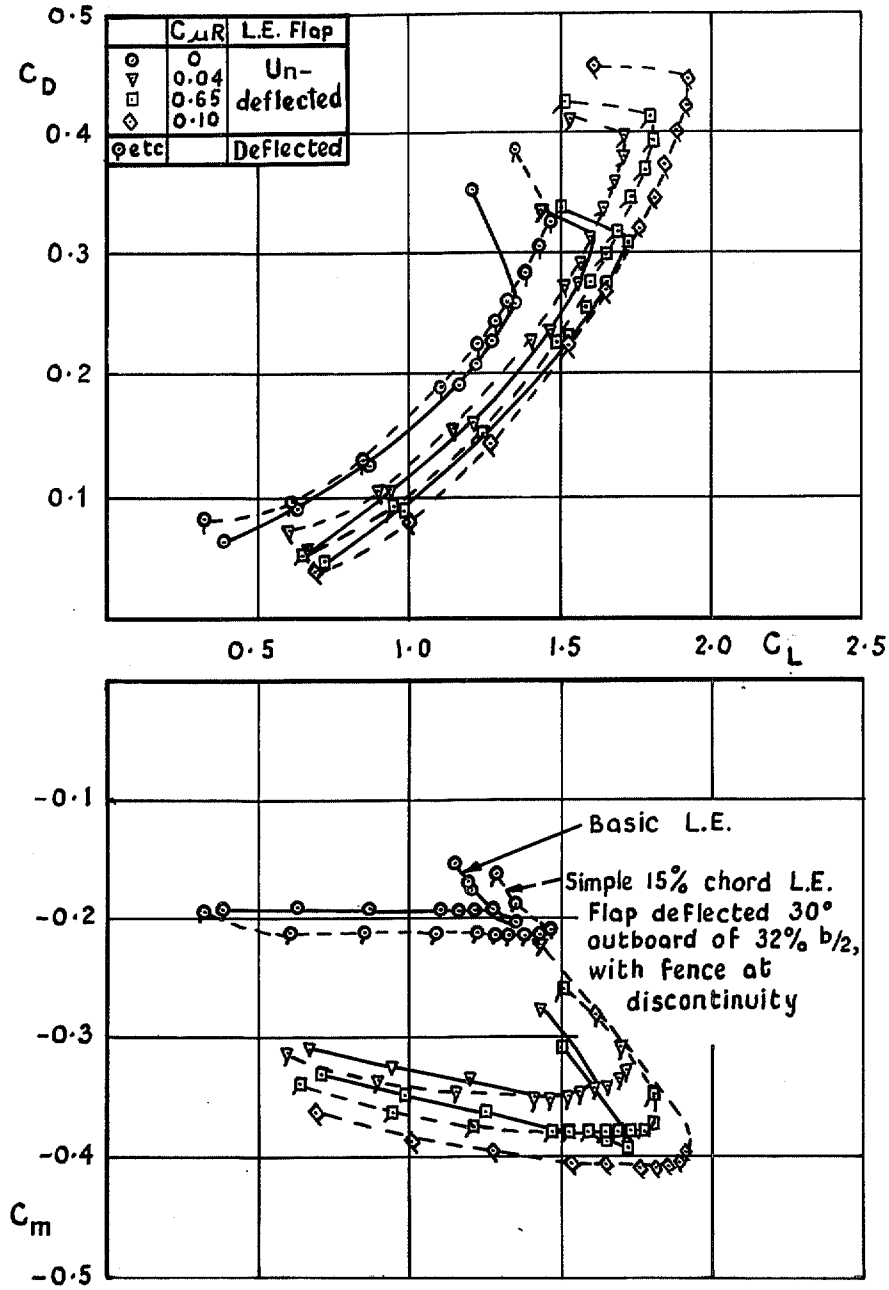

(b)&(c) C_D v C_L & C_m v C_L (no tailplane)

FIG. 13 (*contd.*).

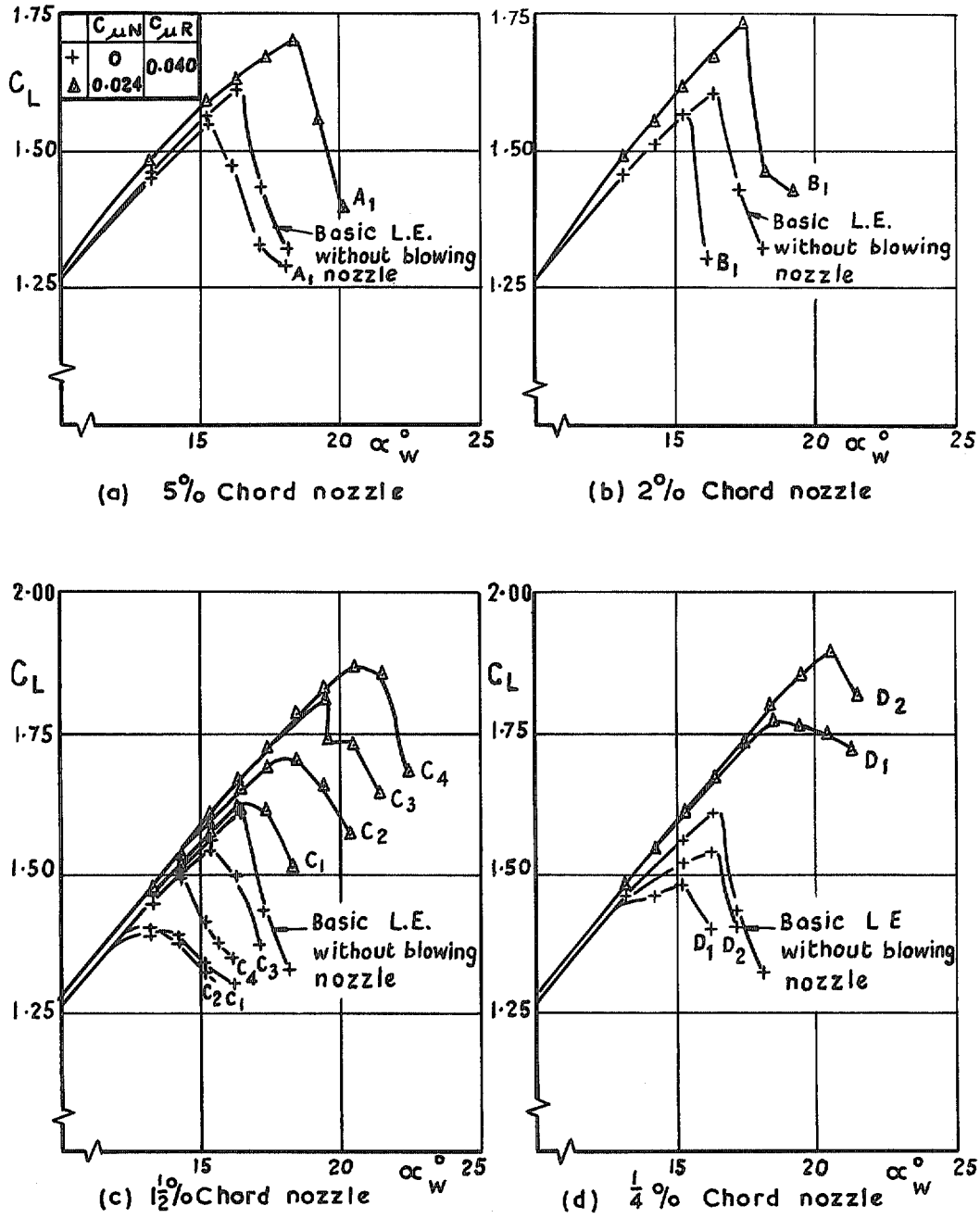

FIG. 14. The effect of L.E. contour and nozzle position on C_L (no tailplane) *vs* α_w. Original L.E. blowing arrangement. $\beta = 30°$, $\xi = 20°$.

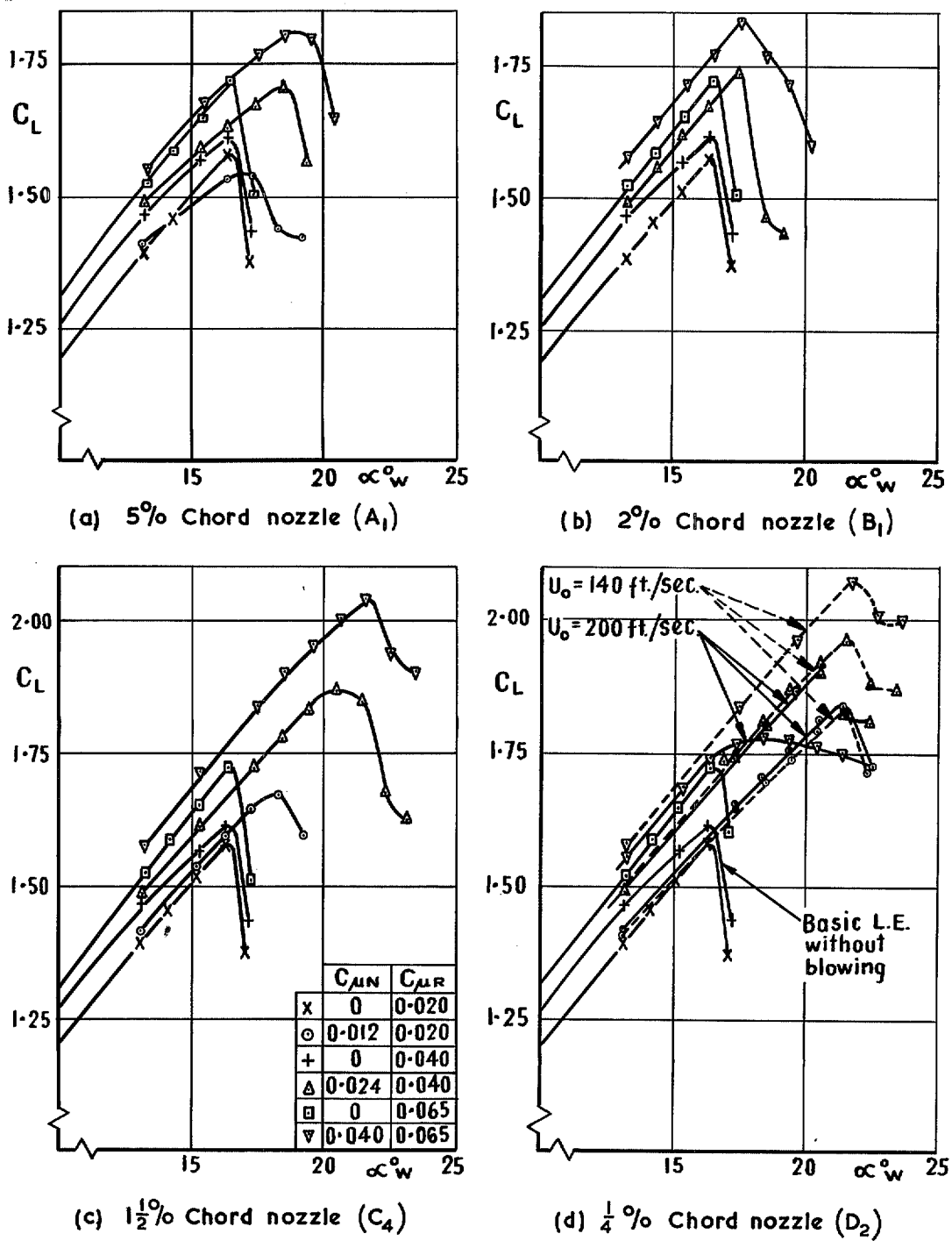

FIG. 15. The effect of L.E. blowing on C_L (no tailplane) *vs* α_w. Original L.E. blowing arrangement. $\beta = 30°$, $\xi = 20°$.

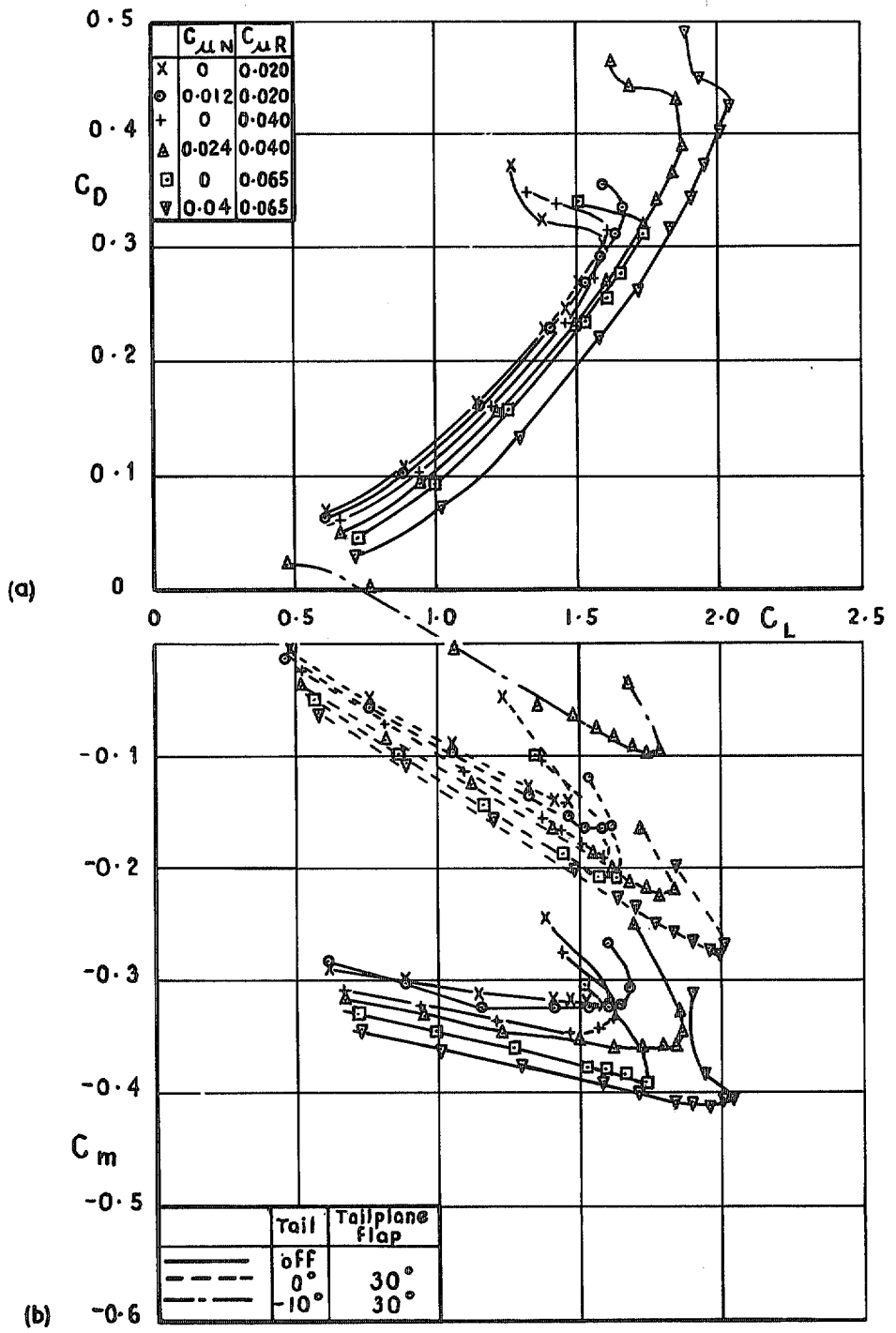

FIG. 16. The effect of L.E. blowing at $1\frac{1}{2}\%$ chord on C_D *vs* C_L (no tailplane) and C_m *vs* C_L. Original L.E. blowing arrangement, configuration C_4.

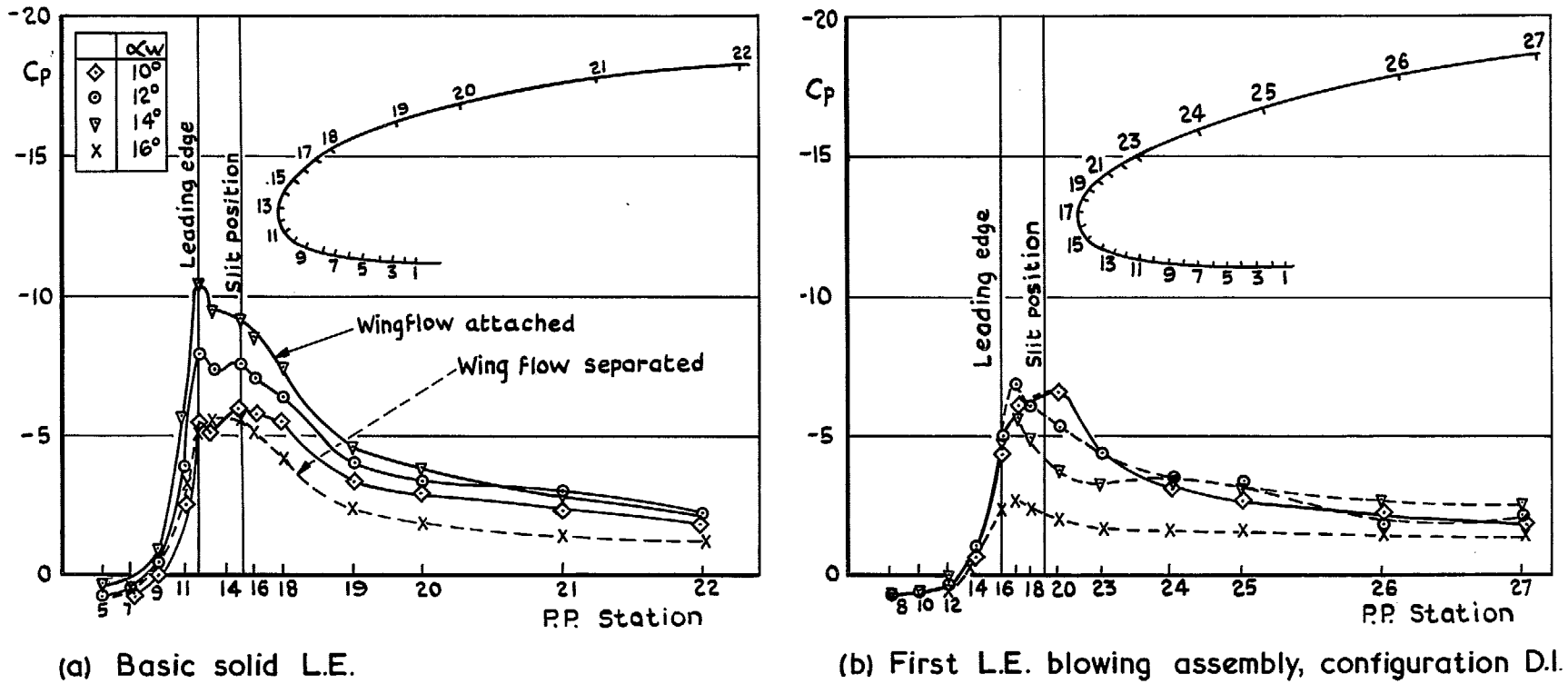

FIG. 17. The effect of L.E. profile on pressure distributions at 75% semi-span, without L.E. blowing.
$\beta = 30°, \xi = 20°$; $C_{\mu_R} = 0{\cdot}04$. $U_0 = 200$ ft/sec.

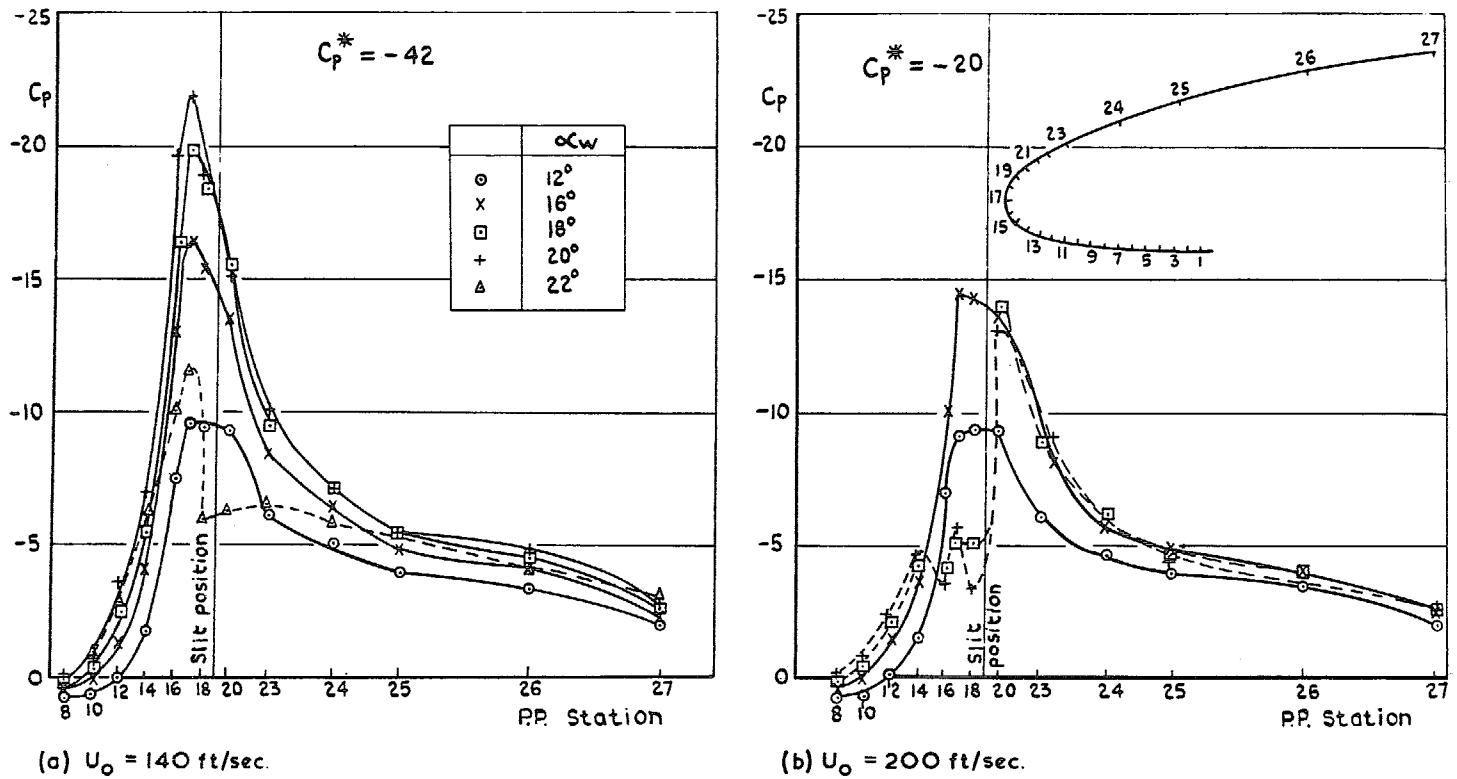

FIG. 18. The effect of main-stream speed on pressure distributions at 75% semispan, with L.E. blowing. Original L.E. arrangement, configuration D_1. $\beta = 30°$, $\xi = 20°$, $C_{\mu_N} = 0{\cdot}024$, $C_{\mu_R} = 0{\cdot}04$.

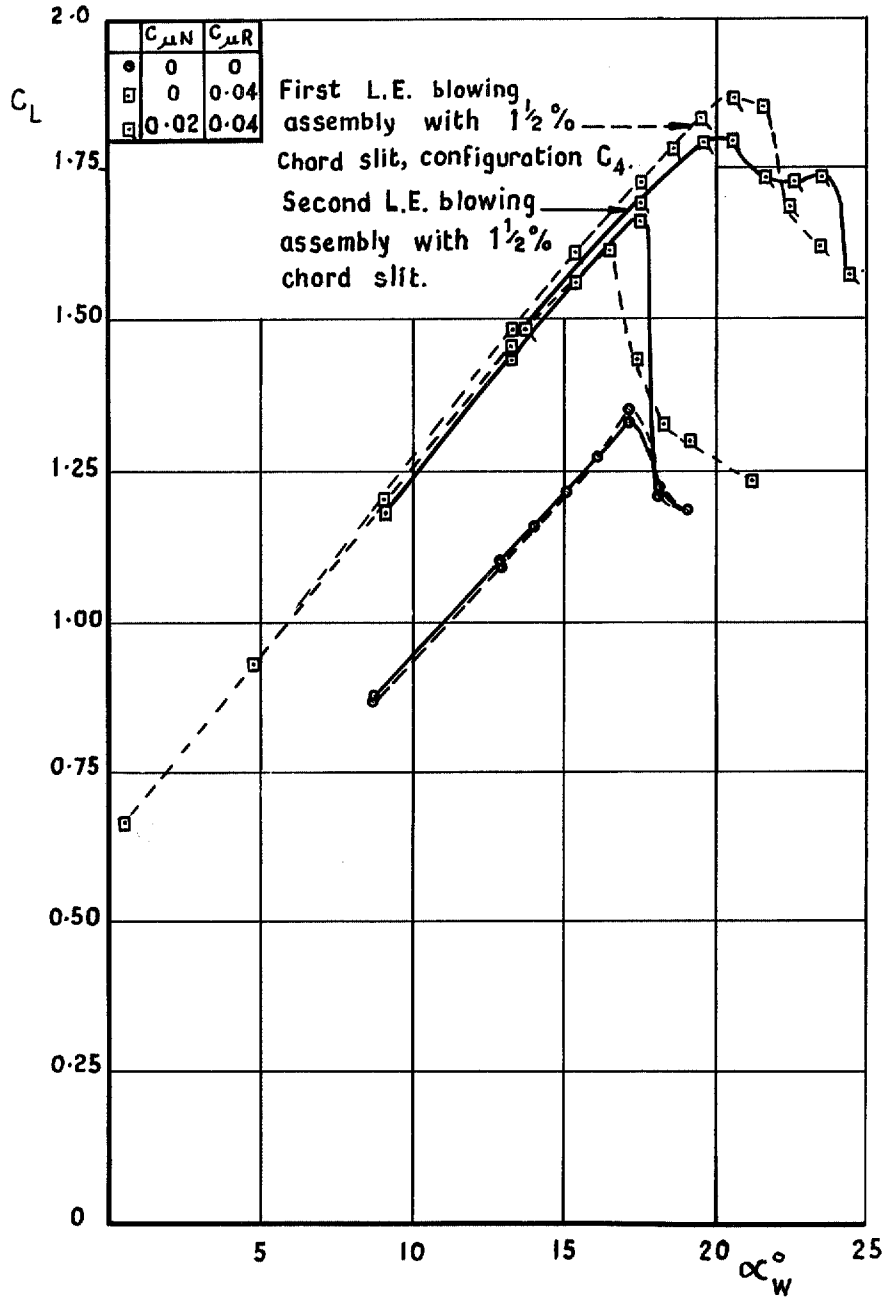

FIG. 19. Comparison between first and second series of tests, with L.E. blowing at $1\frac{1}{2}\%$ chord, $\beta = 30°$, $\xi = 20°$.

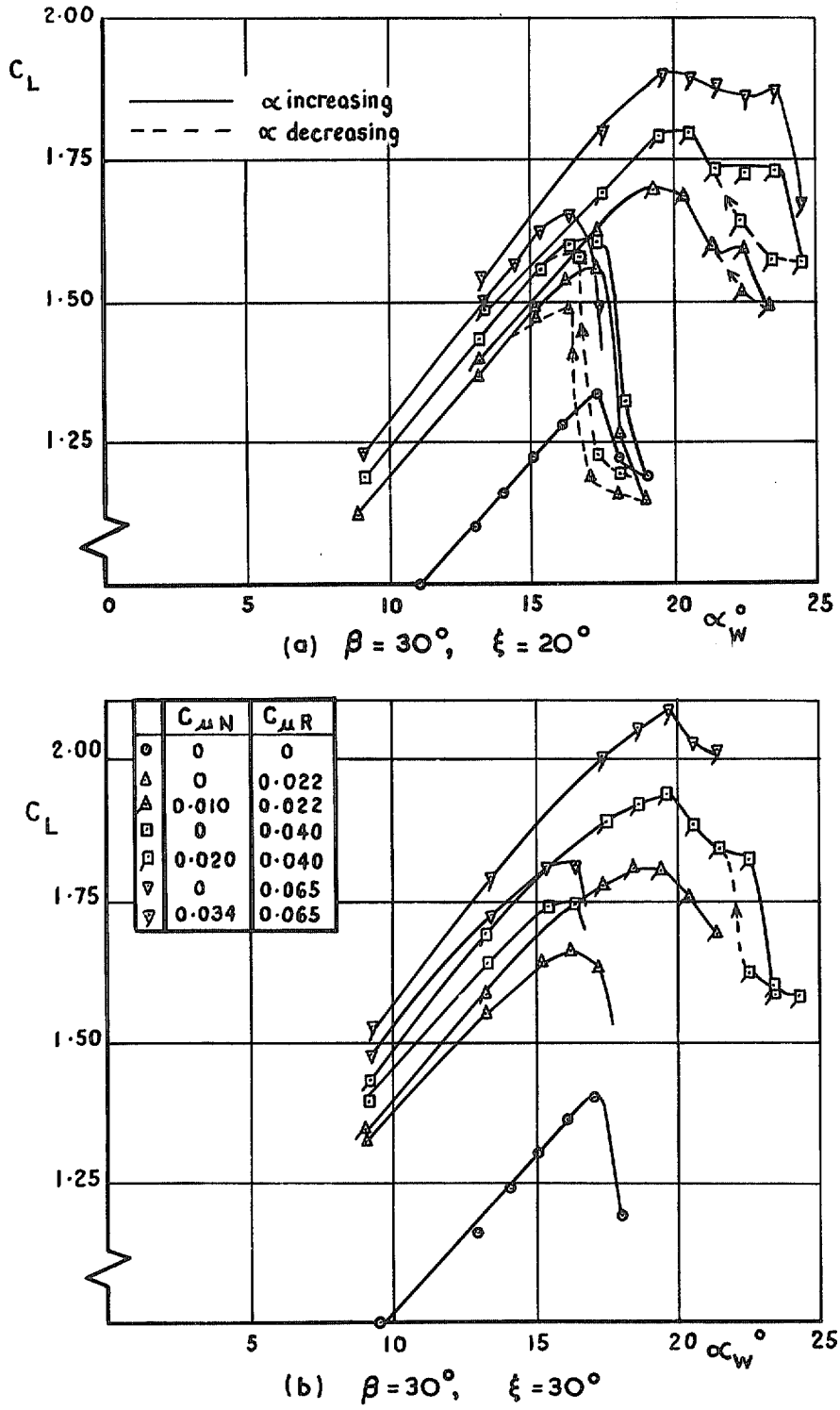

FIG. 20. The combined effect of L.E. and T.E. blowing on C_L (no tailplane) *vs* α_w. Second L.E., with $1\frac{1}{2}\%$ chord nozzle.

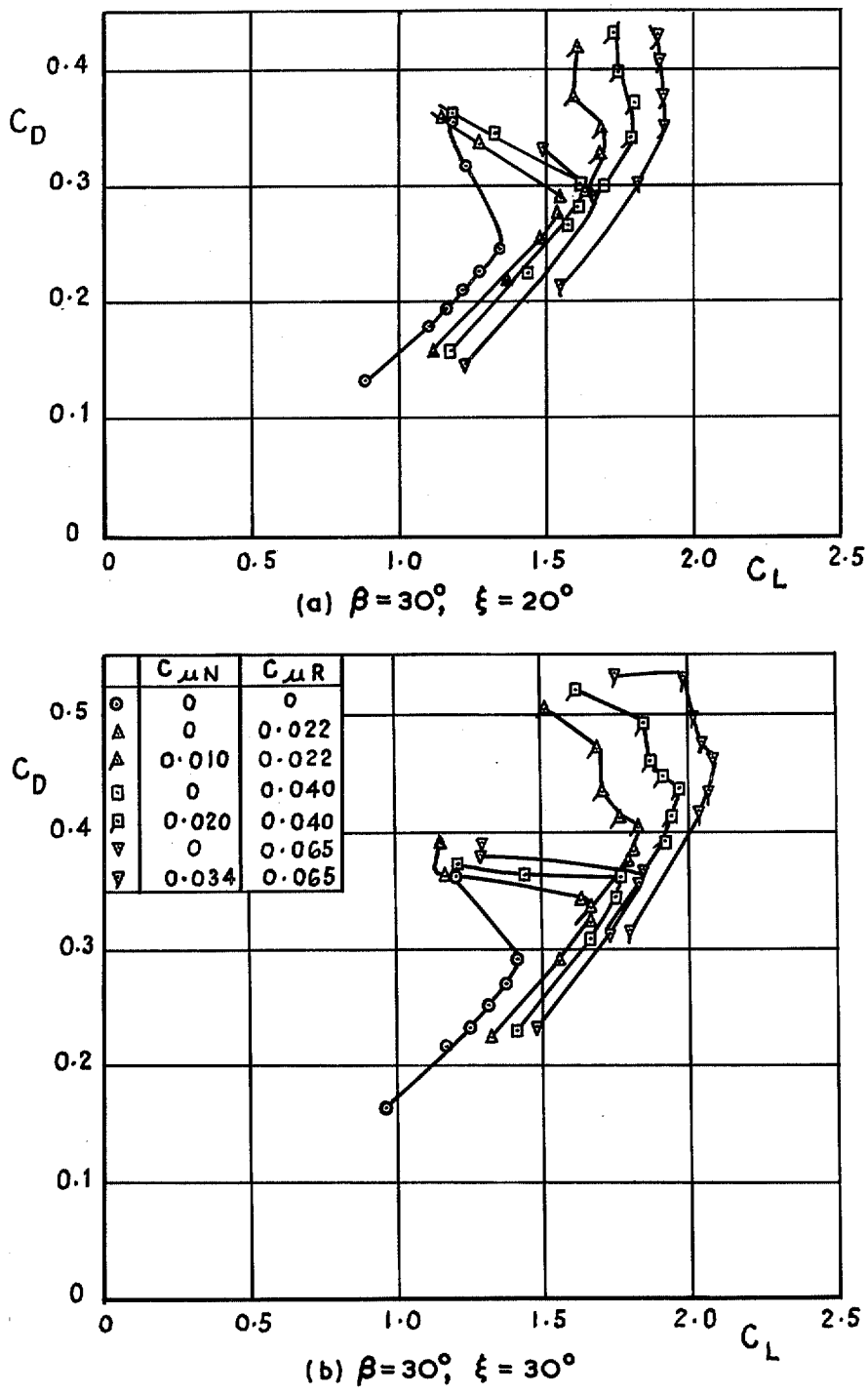

FIG. 21. The combined effect of L.E. and T.E. blowing on C_D *vs* C_L (no tailplane). Second L.E., with $1\frac{1}{2}\%$ chord nozzle.

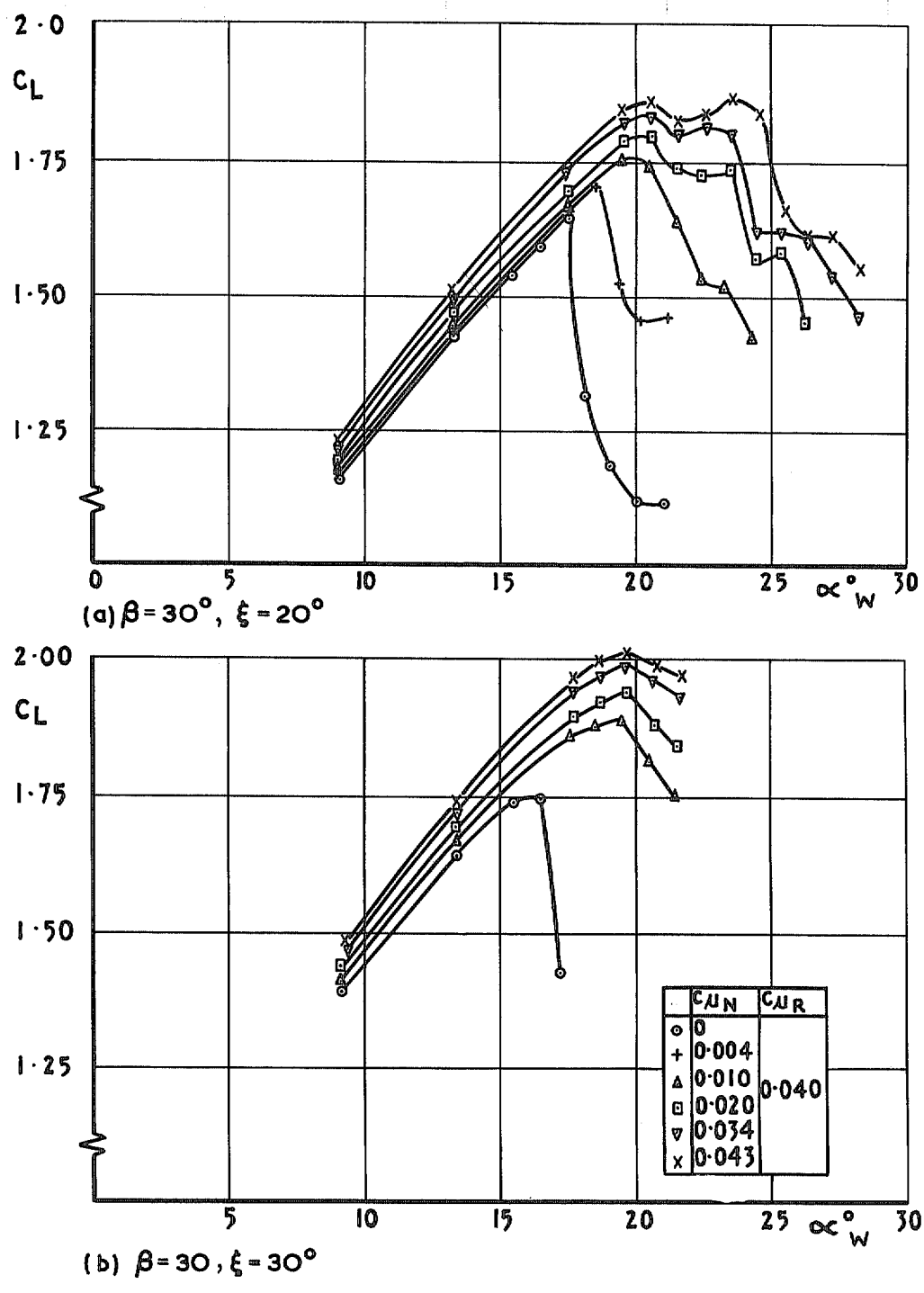

FIG. 22. The effect of L.E. blowing on C_L (no tailplane) *vs* α_w. Second L.E. with $1\frac{1}{2}\%$ chord nozzle.

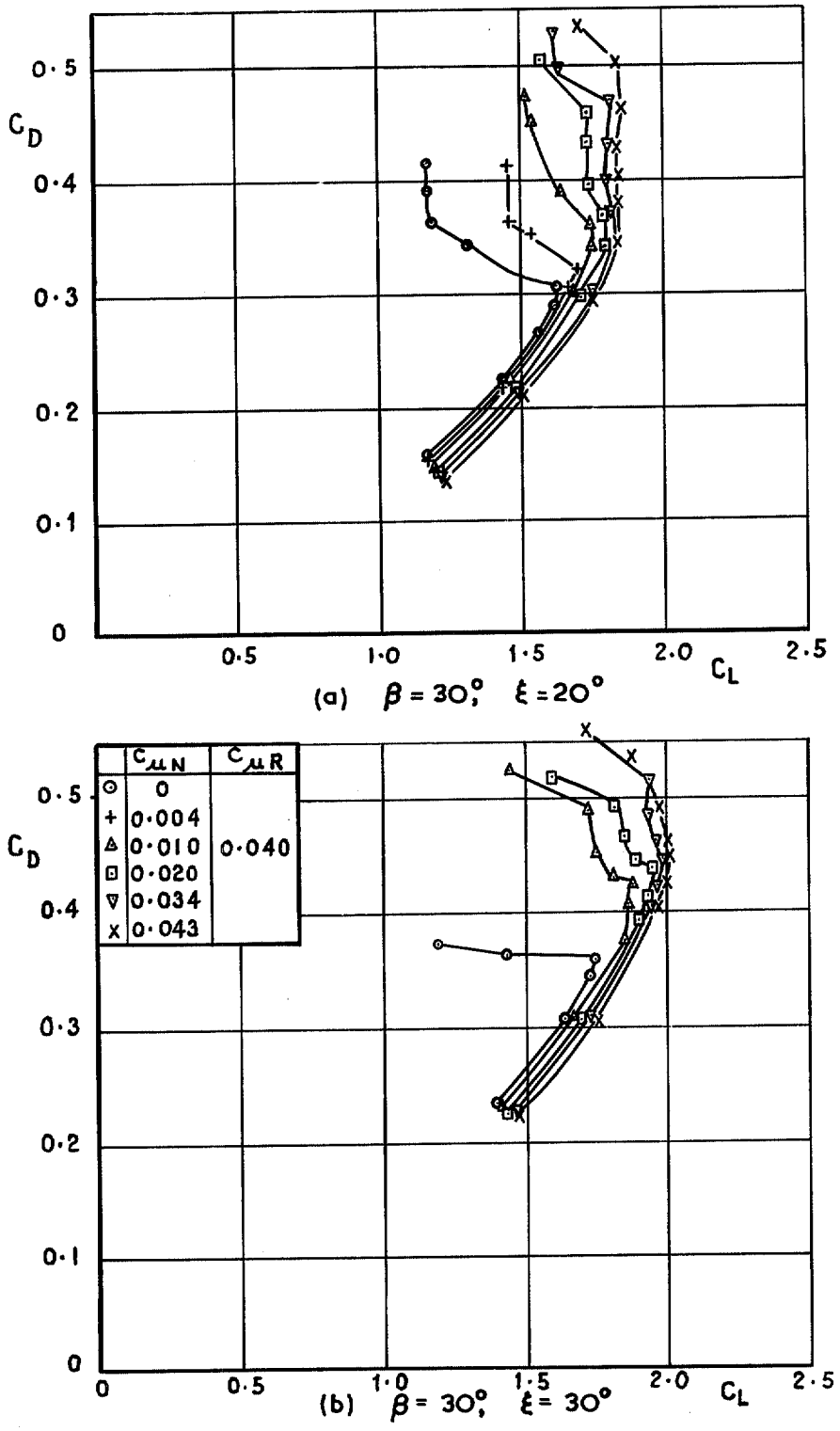

FIG. 23. The effect of L.E. blowing on C_D *vs* C_L (no tailplane). Second L.E. with $1\frac{1}{2}\%$ chord nozzle.

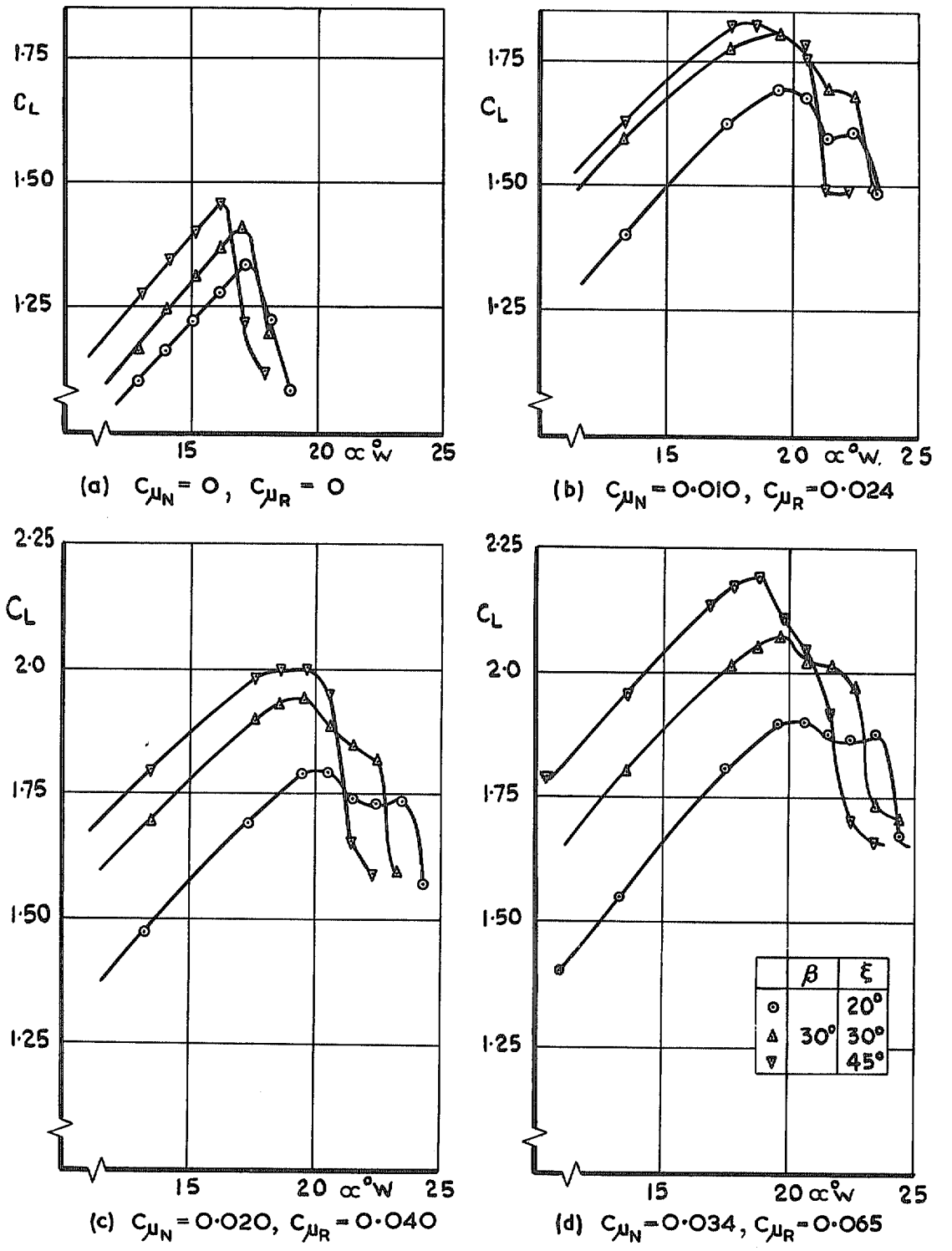

FIG. 24. The combined effect of L.E. and shroud blowing on aileron effectiveness. Second L.E., with $1\frac{1}{2}\%$ chord nozzle.

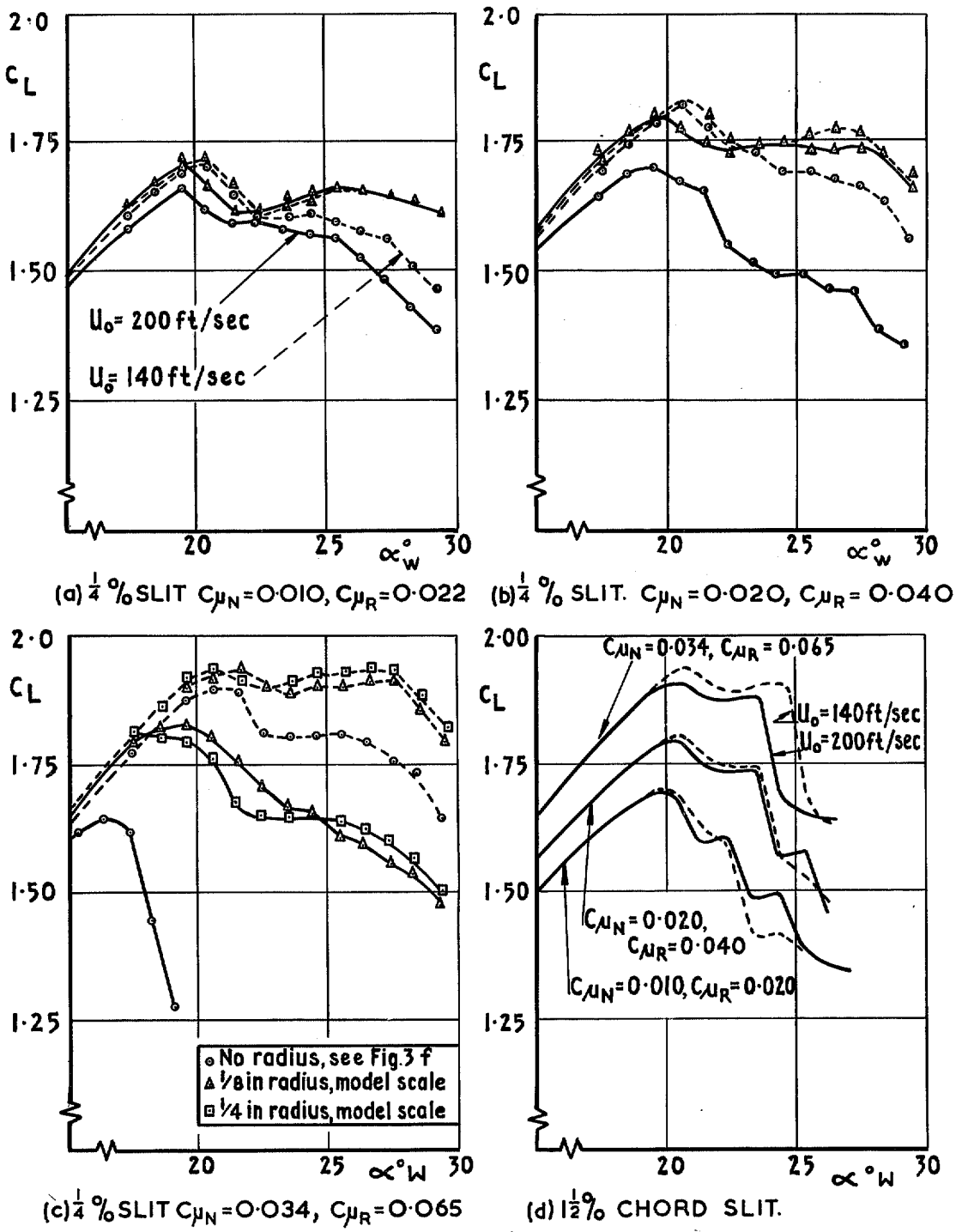

FIG. 25. The effect of L.E. blowing and mainstream speed on C_L (no tailplane) *vs* α_w. Second L.E., with $\frac{1}{4}$% and 1½% chord nozzles.

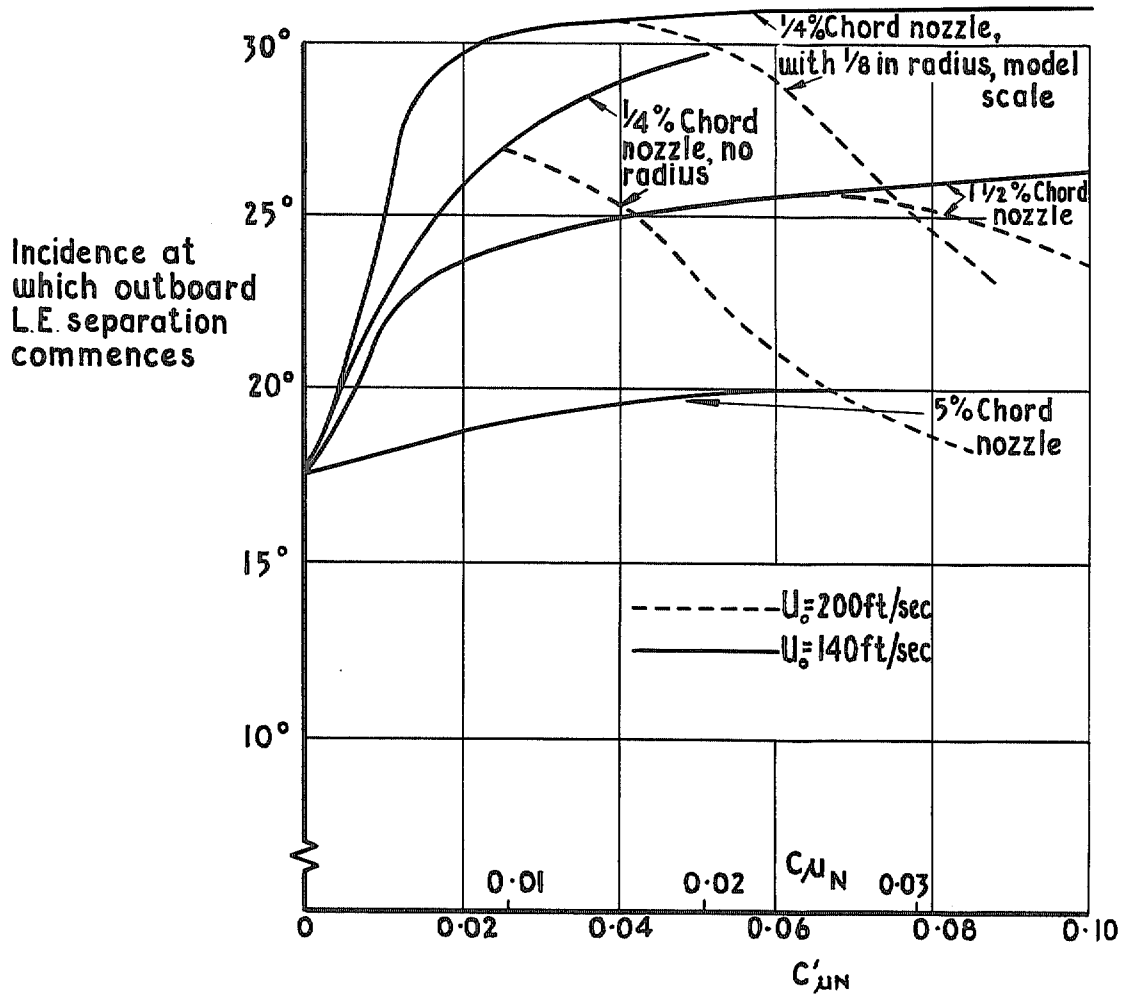

FIG. 26. Wing tuft studies of flow separations from outboard wing. Second L.E., with $\frac{1}{4}$% and $1\frac{1}{2}$% chord nozzles.

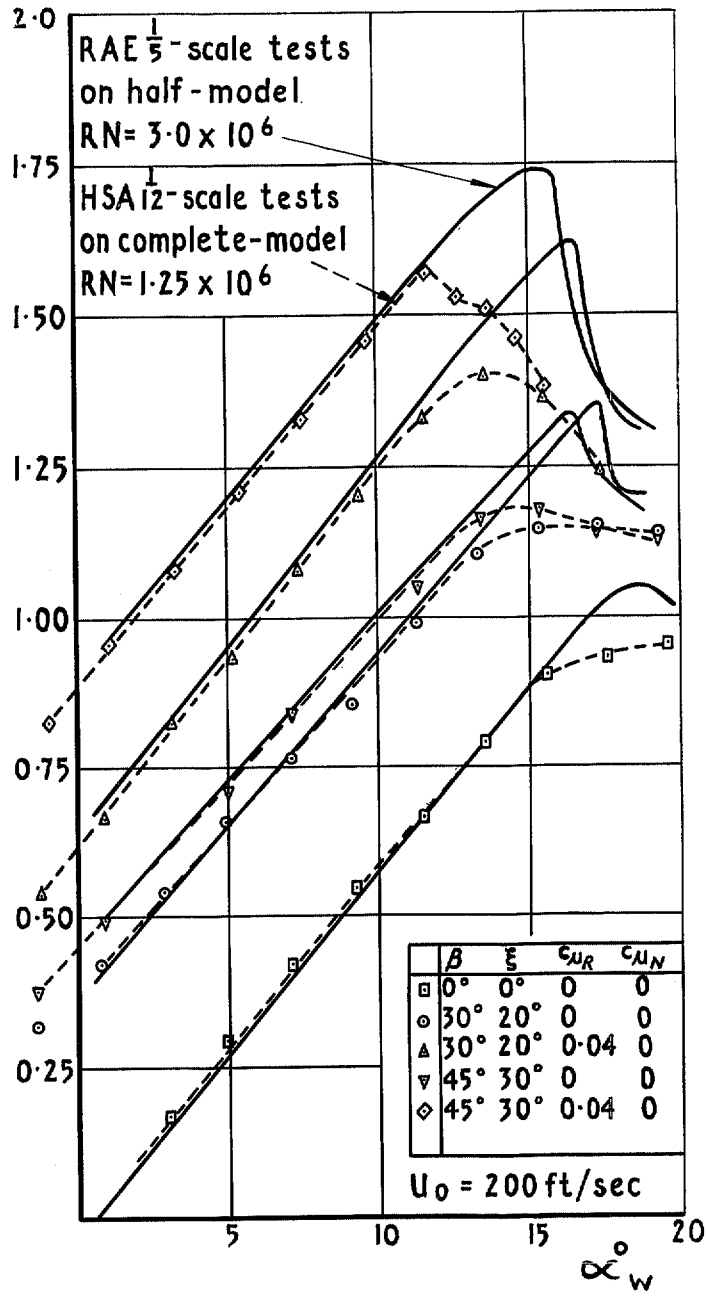

FIG. 27. Comparison with HSA complete-model tests.

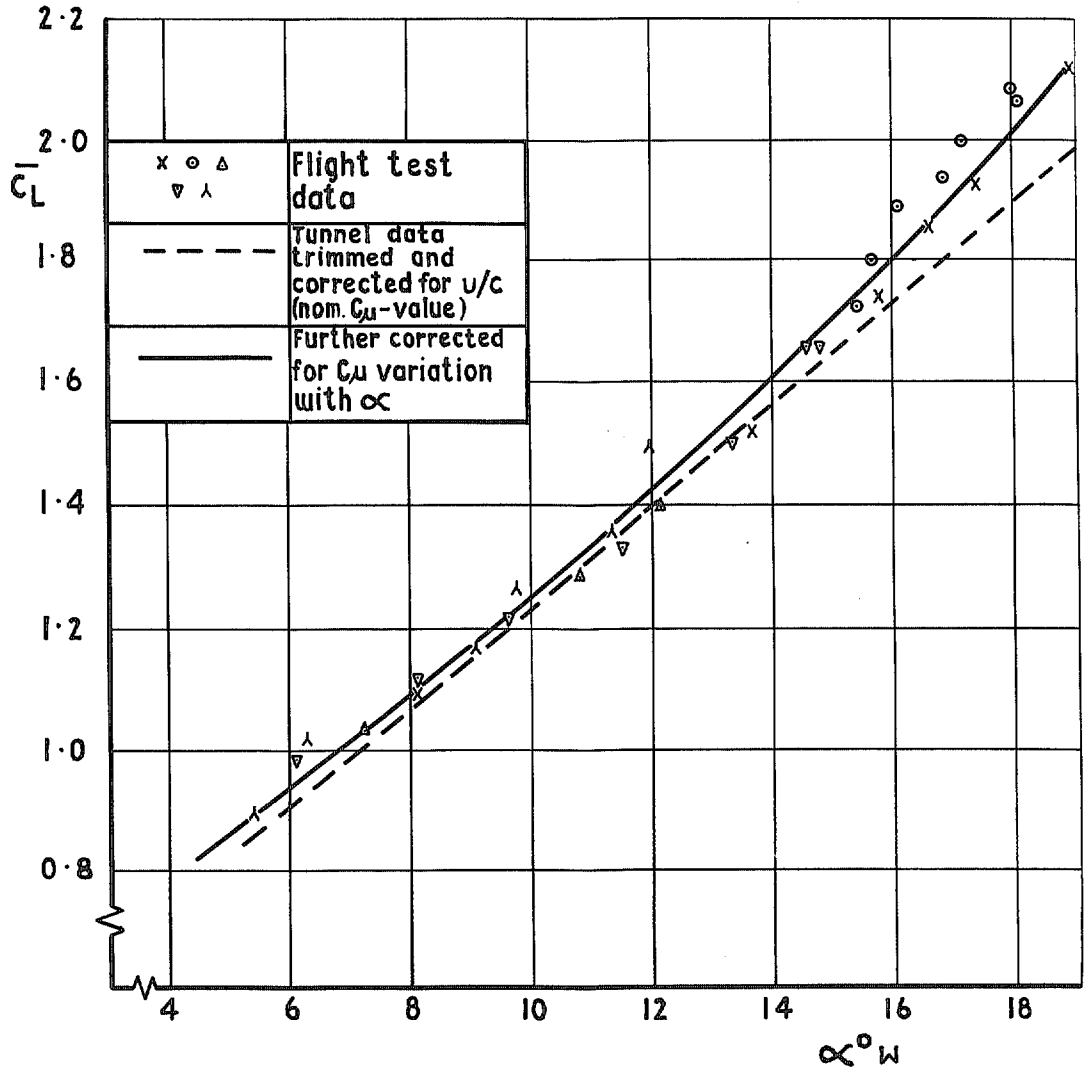

FIG. 28. Flight-tunnel comparison of $\bar{C}_L$ *vs* α_w. $\beta = 45°$, $\xi = 25°$, tailplane flap = 25° undercarriage down, airbrakes closed, no stores.

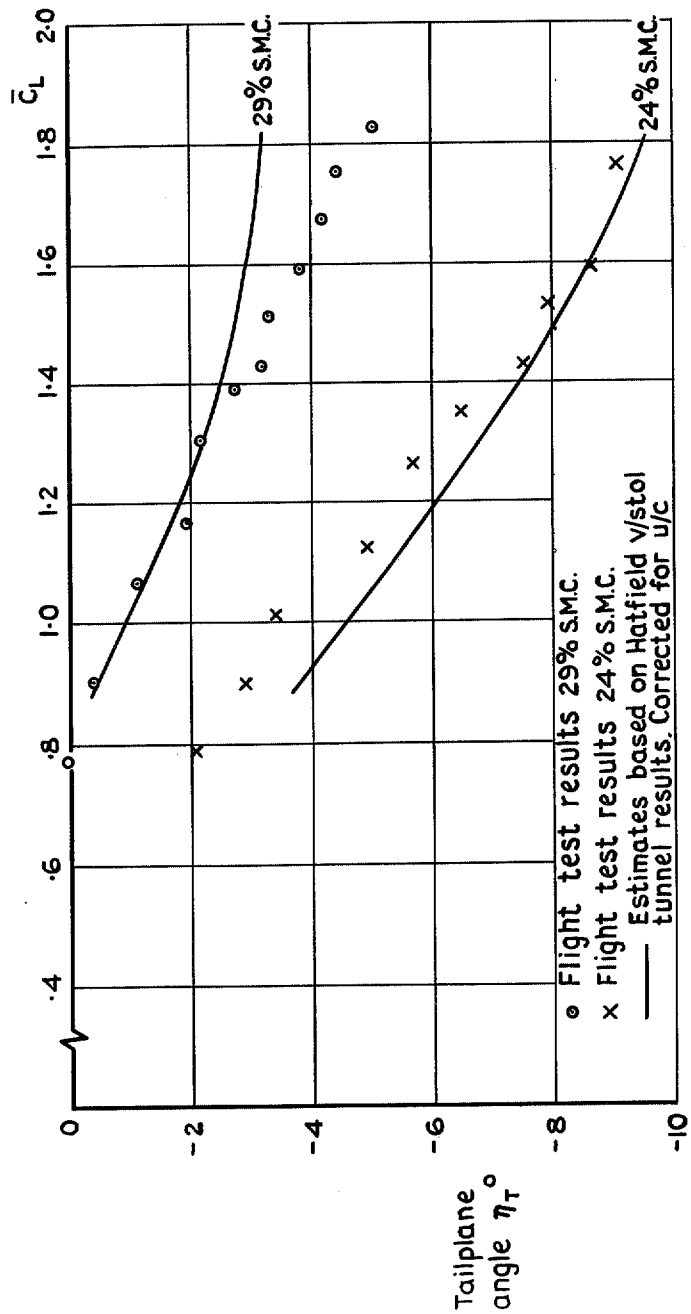

FIG. 29. Flight-tunnel comparison of tailplane angle to trim. $\beta = 45°, \xi = 25°$, tailplane flap = 25° undercarriage down, airbrakes closed, no stores.

Printed in Wales for Her Majesty's Stationery Office by Allens Printers (Wales) Limited

Dd. 501372 K.5

Published by
HER MAJESTY'S STATIONERY OFFICE

To be purchased from
49 High Holborn, London WC1V 6HB
13a Castle Street, Edinburgh EH2 3AR
109 St Mary Street, Cardiff CF1 1JW
Brazennose Street, Manchester M60 8AS
50 Fairfax Street, Bristol BS1 3DE
258 Broad Street, Birmingham B1 2HE
7 Linenhall Street, Belfast BT2 8AY
or through booksellers

R. & M. No. 3655
SBN 11 470375 2